Applications of Deep Learning-Based Probabilistic Approach to Economic Models with High-Dimensional Controls

Hongxiao Chen* and Ji Huang†
The Chinese University of Hong Kong

April 29, 2025

Abstract

In this paper, we combine a deep learning-based probabilistic approach with the finite volume method to numerically solve the equilibrium of economic models with infinite-dimensional controls. We consider two examples to demonstrate the implementation of our method. The first example involves the debt-maturity management problem in a stochastic, time-varying environment, where the infinite-dimensional outstanding debt profile serves as a controlled state variable. In the second example, we explore a preferred habitat model for the term structure of interest rates, where financial intermediaries allocate their portfolios among debt instruments with a continuum of different maturities.

JEL Classification: C63, F34, E43

Keywords: backward stochastic differential equation, deep learning, finite volume method, debt maturity management, term structure of interest rates

*Email:chenhx@link.cuhk.edu.hk

†Contact Details: 9/F Esther Lee Building, The Chinese University of Hong Kong, Shatin, Hong Kong, China. Email:jihuang@cuhk.edu.hk.

Introduction

High-dimensional control problems are commonly encountered in economics, particularly in macroeconomics and finance models involving multiple assets. For instance, when a debt issuer can issue debt across different maturities, the issuer's outstanding debt profile (at various maturities) serves as a critical and high-dimensional state variable. Traditional numerical methods often struggle to compute global solutions when the controlled state variable is high-dimensional. To address this challenge, we propose combining a deep learning-based probabilistic approach with the finite volume method. The former has been applied by the second coauthor to high-dimensional macro-finance models Huang (2023b) and to heterogeneous-agent models with high-dimensional uncontrolled states Huang (2023a), while the latter is a well-established technique in the computational fluid dynamics literature.

We will take a simple example to illustrate the probabilistic formulation and demonstrate the application of deep learning. At the same time, we will highlight the computational challenges posed by high-dimensional control problems. Consider the following dynamic optimization problem, where all variables are assumed to be one-dimensional for simplicity

$$\begin{aligned} V\left(X_t, G_t\right) &= \max_{\alpha_t}: \; u\left(X_t, G_t, \alpha_t\right) + E\left[V\left(X_{t+\Delta}, G_{t+\Delta}\right) \middle| X_t, G_t\right] \\ X_{t+\Delta} &= X_t + \mu\left(X_t, G_t, \alpha_t\right)\Delta + \sigma\left(X_t, G_t, \alpha_t\right)\left(W_{t+\Delta} - W_t\right), \\ G_{t+\Delta} &= G_t + b\left(G_t\right)\Delta + \Sigma\left(G_t\right)\left(W_{t+\Delta} - W_t\right), \end{aligned}$$

where Δ is the length of a period, and $W_{t+\Delta} - W_t$ follows a normal distribution, $N(0, \Delta)$. There are two types of state variables in this problem: a controlled state X_t, whose law of motion depends on the choice variable α_t, and an uncontrolled state G_t. Next, we will demonstrate that the high dimensionality of the controlled state is more problematic than that of the uncontrolled state in terms of numerical computation.

As Δ approaches zero, the recursive formulation above yields the Hamilton-Jacobi-Bellman equation

$$\begin{aligned} 0 = \max_{\alpha} &\left\{ u\left(x_t, g_t, \alpha\right) + V_x \mu\left(x, g, \alpha\right) + \frac{1}{2} V_{xx}\left(x, g, \alpha\right)\sigma^2\left(x, g, \alpha\right) + V_{xg}\sigma\left(x, g, \alpha\right)\Sigma\left(g\right) \right\} \\ &+ V_g b\left(g\right) + \frac{1}{2} V_{gg}\left(\Sigma\left(g\right)\right)^2. \end{aligned}$$

This, in turn, gives rise to the first-order condition (FOC) with respect to α_t

$$\frac{\partial}{\partial \alpha} u\left(x, g, \alpha\right) + V_x \frac{\partial}{\partial \alpha}\mu\left(x, g, \alpha\right) + \frac{1}{2} V_{xx}\left(x, g, \alpha\right)\frac{\partial}{\partial \alpha}\sigma^2\left(x, g, \alpha\right) + V_{xg}\frac{\partial}{\partial \alpha}\sigma\left(x, g, \alpha\right)\Sigma\left(g\right) = 0$$

The FOC indicates that when the dimensionality of the controlled state increases by an order of N, the calculation of the second-order derivatives V_{xx} will increase by an order of N^2. Considering this difficulty, in this paper, we consider a relatively simpler case in which the volatility term of the controlled state is not affected by the choice variable, that is,

$$X_{t+\Delta} = X_t + \mu\left(X_t, G_t, \alpha_t\right)\Delta + \sigma\left(X_t, G_t\right)\left(W_{t+\Delta} - W_t\right). \tag{1}$$

In the simplified version, the HJB equation becomes

$$0 = \max_{\alpha} \{u(x_t, g_t, \alpha) + V_x \mu(x, g, \alpha)\} + \frac{1}{2} V_{xx}(x, g) \sigma^2(x, g, \alpha) + V_{xg} \sigma(x, g) \Sigma(g) + V_g b(g) + \frac{1}{2} V_{gg} (\Sigma(g))^2 .$$

The corresponding FOC is reduced to

$$\frac{\partial}{\partial \alpha} u(x, g, \alpha) + V_x \frac{\partial}{\partial \alpha} \mu(x, g, \alpha) = 0.$$

Under this simplified version, the optimal choice α_t only depends on the first-order derivative, which is still manageable using a deep learning-based probabilistic method. It is worth noting that if we use deep learning to solve the HJB equation directly, the simplification introduced by equation (1) does not help because the numerical calculation of the second-order derivatives V_{xx} remains necessary.

We now introduce the deep learning-based probabilistic approach. By the martingale representation theorem, there exists ψ_t such that, for any realization of $W_{t+\Delta}$, the following relationship holds

$$V(X_{t+\Delta}, G_{t+\Delta}) = V_t - u(X_t, G_t, \hat{\alpha}_t) + \psi_t (W_{t+\Delta} - W_t) .$$

By combining this with the law of motion for X_t and G_t, as well as the first-order condition (FOC), we can define the fixed point $V(x, g)$ and $\psi(x, g)$ in sequence space, where each path in this space corresponds to a realization of $W_{t+\Delta} - W_t$. Based on this formulation, we employ deep learning techniques to solve for the fixed point. Specifically, we use feedforward neural networks to approximate the fixed point, denoted as $\hat{V}(x, g; \Theta)$ and $\hat{\psi}(x, g; \Theta)$, where Θ represents the parameters of the neural network.

To address the high-dimensional state space, we sample as many points in the state space as possible and simulate as many shocks $W_{t+\Delta} - W_t$ as possible. The following loss minimization problem represents the optimization problem that we present to a machine learning package

$$\begin{aligned}
\min_{\Theta} : & \frac{1}{NM} \sum_{i=1}^{N} \sum_{j=1}^{M} \left(\hat{V}\left(\hat{x}^{i,j}, \hat{g}^{i,j}; \Theta\right) + u\left(x^i, g^i, \hat{\alpha}^i\right) \Delta - \hat{V}\left(x^i, g^i; \Theta\right) - \psi\left(x^i, g^i; \Theta\right) w^{i,j} \right)^2 \\
\text{s.t.} \quad & \hat{x}^{i,j} = x^i + \mu\left(x^i, g^i, \hat{\alpha}^i\right) \Delta + \sigma\left(x^i, g^i\right) w^{i,j} \\
& \hat{g}^{i,j} = g^i + b\left(g^i\right) \Delta + \Sigma\left(g^i\right) w^{i,j} \\
& \frac{\partial}{\partial \alpha} u\left(x^i, g^i, \hat{\alpha}^i\right) + \hat{V}_x\left(x^i, g^i; \Theta\right) \frac{\partial}{\partial \alpha} \mu\left(x^i, g^i, \hat{\alpha}^i\right) = 0 \\
& w^{i,j} \text{ is sampled independently from } N(0, \Delta) \\
& x^i, y^i \text{ are from a given set.}
\end{aligned}$$

For certain applications, the controlled states are represented as a continuum. When these states can be indexed by a continuous system, we employ the finite volume method. Specifically, if the state variable is indexed by a continuous parameter, i.e., $X_t(\tau)$, and the function $X_t(\cdot)$ is continuous and remains bounded at the tail (where τ becomes large), we divide the domain

of $X_t(\cdot)$ into finite intervals, denoted as $[\tau^{k-1}, \tau^k]$. Within each interval, the function's value is approximated by a scalar given by

$$X_t^k = \frac{1}{\tau^k - \tau^{k-1}} \int_{\tau^{k-1}}^{\tau^k} X_t(\tau)\, \mathrm{d}\tau.$$

In this way, the function $X_t(\tau)$ is approximated by the step function

$$\sum_{k=1}^{K} X_t^k \mathbf{1}\left\{\tau^{k-1} \leq \tau < \tau^k\right\}$$

The finite volume method differs from the finite difference method, where a finite number of scalars approximate the continuous function at specific grid points. Consequently, the finite volume method is better suited for approximating the original function over its entire domain and more effectively captures the function's transitions over time. Furthermore, the finite volume method remains applicable even if $X_t(\cdot)$ exhibits certain asymptotic properties, such as a Pareto tail, for large values of τ.

To demonstrate our method, we consider two examples involving infinite-dimensional controls. The first example examines a government's debt maturity management problem, as outlined in Bigio, Nuno and Passadore (2023), while the second focuses on the preferred habitat model of the term structure of interest rates, based on Kekre, Lenel and Mainardi (2024). In the first example, the government's outstanding debt profile serves as an infinite-dimensional controlled state variable, which is not influenced by local risks, such as Brownian shocks. We use the finite volume method to characterize its law of motion. In the second example, the controlled state variable is the total wealth of the intermediary sector. Although the wealth variable is one-dimensional, it is affected by Brownian shocks. Moreover, since debt exists across a continuum of maturities, the choice variable is infinite-dimensional. For this case, we apply the finite volume method to characterize the first-order condition.

Literature. The mathematical foundation of our numerical approach is nonlinear Backward Stochastic Differential Equations (BSDEs), which were first developed by mathematicians over three decades ago, beginning with the seminal work of Pardoux and Peng (1990). By integrating this framework with deep learning, applied mathematicians have demonstrated the numerical superiority of BSDEs in solving high-dimensional Partial Differential Equations (Han, Jentzen and E, 2018). Building on these advancements, Huang (2023b,a) introduced a deep learning-based probabilistic approach to the economics literature, showing that all forward-looking stochastic processes, such as asset prices and continuation values, can be represented using BSDEs. Specifically, Huang (2023a) highlights the advantages of the probabilistic formulation for solving models with high-dimensional *uncontrolled* states. Our paper extends this method to address models with high-dimensional *controls* and *controlled* states.

Our paper contributes to the literature on optimal debt maturity management (Angeletos, 2002; Aiyagari, Marcet, Sargent and Seppälä, 2002). Our approach can be applied to enriched extensions of existing models, such as those studied by Lustig, Sleet and Yeltekin (2008), Arellano and Ramanarayanan (2012), Guibaud, Nosbusch and Vayanos (2013), and Faraglia,

Marcet, Oikonomou and Scott (2019), among others. Similar to our work, Valaitis and Villa (2024) leverage modern machine learning techniques to address governments' debt management problems involving three or four types of maturities. In contrast, our method accommodates debt across a continuum of maturities.

The corporate finance literature also examines firms' debt maturity management. For instance, Brunnermeier and Yogo (2009) analyzes how firms dynamically choose between long-term and short-term debt to balance rollover risk and the effective maturity of their liabilities. Similarly, He and Milbradt (2016) investigates a firm's decision to issue two types of long-term bonds with different maturities, aiming to determine its optimal debt maturity structure. Furthermore, DeMarzo and He (2021) studies the optimal debt maturity structure in situations where firms are unable to commit to a future leverage policy.

As our second example demonstrates, our approach can be applied to the literature on the term structure of interest rates. Vayanos and Vila (2021) formalize the framework and investigate how preferred habitat investors and arbitrageurs influence the term structure. Applications of this framework include Gourinchas, Ray and Vayanos (2022), who explore term premia, exchange rates, and monetary policy spillovers in a two-country context, and Ray, Droste and Gorodnichenko (2024), who examine the effects of quantitative easing using Treasury auction data within a preferred habitat model.

The organization of the paper is as follows. Section 1 illustrates the deep learing-based probabilistic approach and the implementation of the finite volume method. In Sections 2, we will demonstrate how to use our method to numerically solve the debt-maturity management problem of a government facing an infinite-dimensional state variable. Section 3 considers the preferred habitat model on the term structure of interest rates, in which financial intermediaries construct their portfolios over a continuum of debt at various maturities. In Section 4, readers can find our remarks on future works.

1 General Method

In this section, we first outline the application of a deep learning-based probabilistic approach to numerically solve a class of high-dimensional control problems. Next, we demonstrate the discretization of a continuum of controls or controlled states using the finite volume method.

1.1 Deep Learning-Based Probabilistic Approach

Consider an agent who maximizes his or her lifetime expected utility function

$$V_0 = \max_{\alpha_t} E_0 \left[\int_0^\infty e^{-\rho s} f\left(X_s, G_s, \alpha_s\right) \mathrm{d}s \right]$$

where ρ is the time discount factor, the $K-$dimensional control variable α_t takes values in a convex set, $X_t \in R^N$ and $G_t \in R^M$ are individual and aggregate state variables, respectively. The law of motion for the individual state is

$$\mathrm{d}X_t = \mu\left(X_t, G_t, \alpha_t\right) \mathrm{d}t + \sigma\left(X_t, G_t\right) \mathrm{d}W_t.$$

For simplicity, we consider the example that the exposure of the individual state to the Brownian shock W_t is not affected by the agent's choice α_t. The aggregate state G_t follows

$$\mathrm{d}G_t = b\left(G_t\right)\mathrm{d}t + \Sigma\left(G_t\right)\mathrm{d}W_t.$$

The Hamilton-Jacobi-Bellman equation of the agent's dynamic programming problem defines the value function $V(x,g)$, i.e.,

$$\begin{aligned}\rho V = \max_{\alpha}\left\{f\left(x,g,\alpha\right) + \nabla_x V\cdot\mu\left(x,g,\alpha\right)\right\} + \frac{1}{2}\mathrm{tr}\left(\sigma\left(x,g\right)^T\nabla_{xx}V\ \sigma\left(x,g\right)\right)\\ + \nabla_g V\cdot b\left(g\right) + \frac{1}{2}\mathrm{tr}\left(\Sigma\left(g\right)^T\nabla_{gg}V\ \Sigma\left(g\right)\right),\end{aligned}$$

where $\cdot$ denotes inner product, $\mathrm{tr}\left(\cdot\right)$ represents the trace operator, and ^{T} denotes transpose. The first-order condition w.r.t α_t is

$$0 = \nabla_\alpha f\left(X_t,G_t,\hat{\alpha}_t\right) + \nabla_\alpha\left(\nabla_x V\cdot\mu\left(X_t,G_t,\hat{\alpha}_t\right)\right).$$

Taking the optimal choice $\hat{\alpha}_t$ that is Markovian in state variables (X_t,G_t) as given, we next derive the BSDE that defines the value function $V\left(x,g\right)$. We first construct a martingale

$$\int_0^t e^{-\rho s}f\left(X_s,G_s,\hat{\alpha}_s\right)\mathrm{d}s + e^{-\rho t}V_t = E_t\left[\int_0^\infty e^{-\rho s}f\left(X_s,G_s,\hat{\alpha}_s\right)\mathrm{d}s\right].$$

The martingale representation theorem implies that there exists an adapted process ψ_t^V such that

$$\int_0^t e^{-\rho s}f\left(X_s,G_s,\hat{\alpha}_s\right)\mathrm{d}s + e^{-\rho t}V_t = V_0 + \int_0^t e^{-\rho s}\psi_s^V\mathrm{d}W_s,$$

whose differential form yields the BSDE

$$\begin{aligned}e^{-\rho t}f\left(X_t,G_t,\hat{\alpha}_t\right)\mathrm{d}t - \rho e^{-\rho t}V_t\mathrm{d}t + e^{-\rho t}\mathrm{d}V_t &= e^{-\rho t}\psi_t^V\mathrm{d}W_t\\ \mathrm{d}V_t &= -\left(f\left(X_t,G_t,\hat{\alpha}_t\right) - \rho V_t\right)\mathrm{d}t + \psi_t^V\mathrm{d}W_t.\end{aligned}$$

The predictability means the realization of ψ_t^V is fully determined based on the information available *right before* time t.

The Forward-Backward SDE system that defines the value function $V\left(x,g\right)$ along with the volatility term $\psi^V\left(x,g\right)$ is

$$\begin{aligned}\mathrm{d}V_t &= -\left(f\left(X_t,G_t,\hat{\alpha}_t\right) - \rho V_t\right)\mathrm{d}t + \psi^V\left(X_t,G_t\right)\mathrm{d}W_t\\ \mathrm{d}X_t &= \mu\left(X_t,G_t,\hat{\alpha}_t\right)\mathrm{d}t + \sigma\left(X_t,G_t\right)\mathrm{d}W_t\\ \mathrm{d}G_t &= b\left(G_t\right)\mathrm{d}t + \Sigma\left(G_t\right)\mathrm{d}W_t\\ 0 &= \nabla_\alpha f\left(X_t,G_t,\hat{\alpha}_t\right) + \nabla_\alpha\left(\nabla_x V\cdot\mu\left(X_t,G_t,\hat{\alpha}_t\right)\right)\\ V_t &= V\left(X_t,G_t\right).\end{aligned}$$

The predictability of the process ψ_t^V is equivalent to the existence of function $\psi^V(\cdot,\cdot)$ such that $\psi_t^V = \psi(X_t,G_t)$, which means the realization of ψ_t^V is independent of the innovation $W_{t+\Delta} - W_t$.

Remark 1. The FBSDE system above defines a fixed point in the sequence space, just as the recursive formulation defines one in the state space. Starting from any initial state (X_0, G_0), the fixed point yields the initial value $V_0 = V(X_0, G_0)$. For each realized path of the Brownian shock, the FBSDE system generates a path X_t, G_t, V_t. Moreover, along this path, the fixed point must hold everywhere, i.e., $V_t = V(X_t, G_t)$. A key advantage of the probabilistic formulation is that it eliminates the need to calculate the first- and second-order derivatives of the value function with respect to the *uncontrolled* states G_t and the second-order derivatives with respect to the controlled state X_t. The trade-off, however, is the need to approximate an additional function $\psi^V(x, g)$, whose dimensionality increases with that of the Brownian shock W_t.

Remark 2. If the agent's choice α_t affects the exposure of the controlled state to the Brownian shock, the HJB equation becomes

$$\begin{aligned}\rho V = \max_{\alpha} \left\{ f(x, g, \alpha) + \nabla_x V \cdot \mu(x, g, \alpha) + \frac{1}{2}\text{tr}\left(\sigma(x, g, \alpha)^T \nabla_{xx} V \ \sigma(x, g, \alpha)\right) \right\} \\ + \nabla_g V \cdot b(g) + \frac{1}{2}\text{tr}\left(\Sigma(g)^T \nabla_{gg} V \ \Sigma(g)\right),\end{aligned}$$

and the first-order condition will also involve the Hessian matrix of the value function, $V(x, g)$, with respect to X_t. This implies that the numerical calculation of the high-dimensional second-order derivative is *unavoidable*, which presents a significant challenge, as the number of second-order derivative calculations is of the order N^2.

1.2 Numerical Scheme

We use feedforward neural networks to approximate the value function $\hat{V}(x, g; \Theta)$ and the volatility term $\hat{\psi}^\eta(x, g; \Theta)$. Given an arbitrary T, we discretize the time interval $[0, T]$ evenly as $0 = t_0 < t_1 < t_2 < \cdots < t_n = T$, and simulate M sample paths of Brownian motions, $\{W_{i,m}\}\, m = 1^M$, as well as initial states, $\{x0, m, g_{0,m}\}\, m = 1^M$. The subscript m will be dropped without loss of generality. Let $\Delta \equiv ti + 1 - t_i$ and $w_i = W_{i+1} - W_i$. Initialize $v_0 = \hat{V}(x_0, g_0; \Theta)$. Next, we repeat the following steps for $i = 0$ to $i = n - 1$.

1. Calculate $\nabla_x \hat{V}(x_i, g_i; \Theta)$ with automatic differentiation and $\psi_i^V = \hat{\psi}^V(x_i, g_i; \Theta)$
2. Use the FOC to compute $\hat{\alpha}_i$
3. Calculate v_{i+1}, x_{i+1}, and g_{i+1} according to

$$\begin{aligned} v_{i+1} &= v_i - \left(f(x_i, g_i, \hat{\alpha}_i) - \rho v_i\right)\Delta + \psi_i^V w_i \\ x_{i+1} &= x_i + \mu(x_i, g_i, \hat{\alpha}_i)\,\Delta + \sigma(x_i, g_i)\, w_i \\ g_{i+1} &= g_i + b(g_i)\,\Delta + \Sigma(g_i)\, w_i \end{aligned}$$

4. Compute $\tilde{v}_{i+1} = \hat{v}(x_{i+1}, g_{i+1}; \Theta)$

Given the simulated paths, the loss function is constructed as follows

$$\text{Loss}\left(\Theta; \{x_{0,m}, g_{0,m}, w_{i,m}\}_{i=1,m=1}^{n-1,M}\right) = \frac{1}{Mn}\sum_{m=1}^{M}\sum_{i=1}^{n-1} \|v_i - \tilde{v}_i\|^2,$$

where $\|\cdot\|$ denotes the square norm.

1.3 Infinite-Dimensional Controls and Finite Volume Method

The probabilistic formulation and the numerical scheme presented above address only models with finite-dimensional controls or controlled states. However, in some cases, there is a continuum of controls or controlled states. To handle these, we employ the finite volume method to approximate the infinite-dimensional variables with finite-dimensional ones, enabling the application of the numerical scheme described above.

The finite volume method is widely used in both research and industrial applications of computational fluid dynamics. Its key idea is to approximate a continuous function using a step function. Consider an infinite-dimensional state variable X_t with a continuous index τ, denoted as $X_t(\tau)$. To apply the finite volume method, the domain of $X_t(\cdot)$ is divided into K subintervals, defined by $-\infty < \tau^0 < \tau^1 < \cdots < \tau^K < \infty$, where the boundary points $\tau^k, k = 0, 1, \cdots, K$ are not required to be evenly spaced. For each subinterval $\left[\tau^{k-1}, \tau^k\right]$, we define

$$X_t^k = \frac{1}{\tau^k - \tau^{k-1}} \int_{\tau^{k-1}}^{\tau^k} X_t(\tau)\, \mathrm{d}\tau$$

and the function $X_t(\tau)$ is approximated by the step function

$$\sum_{k=1}^{K} X_t^k \mathbf{1}\left\{\tau^{k-1} \leq \tau < \tau^k\right\}.$$

Remarks. If the index of $X_t(\cdot)$ is unbounded, the finite volume method remains applicable, provided that the function exhibits certain asymptotic properties as τ approaches positive or negative infinity. To enhance the precision of the finite volume method, more intervals can be allocated in regions where the curvature of $X_t(\tau)$ is relatively high. The finite volume method is also versatile enough to accommodate multi-dimensional indices of the state variable X_t and various shapes of cells, which serve as counterparts to intervals in higher dimensions.

In this section, we analyze two special cases for the application of the finite volume method. In the first case, we examine an infinite-dimensional controlled state, wherein the law of motion depends on its local properties—specifically, the dynamics of $X_t(\hat{\tau})$ rely solely on the properties within the neighborhood of $\hat{\tau}$. In the second case, we focus on a one-dimensional controlled state, where the volatility term also depends on the choice variable.

1.3.1 Infinite-dimensional Controlled State

Suppose the utility flow function at time t is

$$u\left(\int_0^{\infty} f\left(X_t, G_t, \tau\right) \alpha_t(\tau)\, \mathrm{d}\tau\right)$$

and the law of motion for $X_t(\tau)$ is

$$\mathrm{d}X_t(\tau) = \left(\mu\left(X_t(\tau), G_t, \alpha_t(\tau)\right) + \frac{\partial}{\partial \tau} X_t(\tau)\right)\mathrm{d}t.$$

The first component of $X_t(\tau)$'s drift depends on $X_t(\tau)$ and $\alpha_t(\tau)$, rather than the entire functions of either $X_t(\cdot)$ or $\alpha_t(\cdot)$. The second component, the partial differential term, implies the local property of $X_t(\cdot)$ around τ also affects the dynamics of $X_t(\tau)$. The first-order condition w.r.t $\alpha_t(\tau)$ is

$$u'(\cdot) f\left(X_t, G_t, \tau\right) + \frac{\partial}{\partial X(\tau)} V_t \frac{\partial}{\partial \alpha(\tau)} \mu\left(X_t(\tau), G_t, \alpha_t(\tau)\right) = 0.$$

To apply the finite volume method, we use the $K-$dimensional stochastic process $\left\{X_t^k\right\}_{k=1}^K$ to approximate $X_t(\tau)$. To derive the law of motion for X_t^k, we integrate over interval $\left[\tau^{k-1}, \tau^k\right]$

$$\mathrm{d}\int_{\tau^{k-1}}^{\tau^k} X_t(\tau)\,\mathrm{d}\tau = \left(\int_{\tau^{k-1}}^{\tau^k} \mu\left(X_t(\tau), G_t, \alpha_t(\tau)\right)\mathrm{d}\tau + X_t\left(\tau^k\right) - X_t\left(\tau^{k-1}\right)\right)\mathrm{d}t.$$

This leads to the following equations

$$\begin{aligned}
\mathrm{d}\left(\tau^k - \tau^{k-1}\right) X_t^k &= \left(\left(\tau^k - \tau^{k-1}\right)\mu\left(X_t(\tau), G_t, \hat{\alpha}_t^k\right) + X_t^{k+1} - X_t^k\right)\mathrm{d}t \\
\mathrm{d}X_t^k &= \left(\mu\left(X_t^k, G_t, \hat{\alpha}_t^k\right) + \frac{X_t^{k+1} - X_t^k}{\tau^k - \tau^{k-1}}\right)\mathrm{d}t,
\end{aligned}$$

where

$$\hat{\alpha}_t^k \equiv \alpha_t\left(\hat{\tau}^k\right), \text{ where } \hat{\tau}^k = 0.5\left(\tau^k + \tau^{k-1}\right)$$

Given the discretization, we focus on the first-order condition at the midpoint of the interval $\left[\tau^{k-1}, \tau^k\right]$

$$u'(\cdot) f\left(X_t, G_t, \hat{\tau}^k\right) + \frac{\partial}{\partial X\left(\hat{\tau}^k\right)} V_t \frac{\partial}{\partial \hat{\alpha}_t^k} \mu\left(X_t\left(\hat{\tau}^k\right), G_t, \hat{\alpha}_t^k\right) = 0$$

1.3.2 Low-Dimensional Controlled State

For simplicity, suppose the utility flow is independent of the control variable, that is,

$$f(x, g),$$

and the law of motion for the one-dimensional state variable X_t is given by

$$\mathrm{d}X_t = \left(\int_0^\infty \mu\left(X_t, G_t, \tau\right)\alpha_t(\tau)\,\mathrm{d}\tau\right)\mathrm{d}t + \left(\int_0^\infty \sigma\left(X_t, G_t, \tau\right)\alpha_t(\tau)\right)\mathrm{d}W_t.$$

Since the volatility term of the controlled state X_t depends on control $\alpha_t(\tau)$, the HJB equation becomes

$$\rho V = \max_{\alpha(\cdot)} \left\{ f(x,g) + V_x \int_0^\infty \mu(X_t, G_t, \tau)\, \alpha_t(\tau)\, \mathrm{d}\tau + \frac{1}{2} V_{xx} \left(\int_0^\infty \sigma(X_t, G_t, \tau)\, \alpha_t(\tau) \right)^2 \right\} + \nabla_g V \cdot b(g) + \frac{1}{2} \mathrm{tr}\left(\Sigma(g)^T \nabla_{gg} V\, \Sigma(g) \right).$$

The first-order condition w.r.t. $\alpha_t(\tau)$

$$V_x \mu(X_t, G_t, \tau) + V_{xx} \sigma(X_t, G_t, \tau) \left(\int_0^\infty \sigma(X_t, G_t, \tau)\, \hat{\alpha}_t(\tau) \right) = 0$$

Given the discretization of the finite volume method, the law of motion for X_t becomes

$$\mathrm{d}X_t = \sum_{k=1}^K \mu^k(X_t, G_t)\, \hat{\alpha}_t^k \left(\tau^k - \tau^{k-1} \right) \mathrm{d}t + \left(\sum_{k=1}^K \sigma^k(X_t, G_t)\, \hat{\alpha}_t^k(\tau) \left(\tau^k - \tau^{k-1} \right) \right) \mathrm{d}W_t, \text{ where}$$
$$\mu^k(X_t, G_t) \equiv \mu\left(X_t, G_t, \hat{\tau}^k \right), \sigma^k(X_t, G_t) \equiv \sigma\left(X_t, G_t, \hat{\tau}^k \right),$$

and the first-order condition is given by

$$V_x \mu(X_t, G_t, \tau) + V_{xx} \sigma(X_t, G_t, \tau) \left(\sum_{k=1}^K \sigma\left(X_t, G_t, \hat{\tau}^k \right) \hat{\alpha}_t\left(\hat{\tau}^k \right) \left(\tau^k - \tau^{k-1} \right) \right) = 0.$$

2 Debt-Maturity Management

In this section, we consider an example of debt maturity management based on Bigio, Nuno and Passadore (2023), where a government issues debt at different maturities while incurring issuance costs due to price impacts. In this example, we allow for a stochastic risk-free interest rate driven by a diffusion process, whereas it is assumed to be constant in Bigio et al. (2023). Consequently, the profile of the government's outstanding debt becomes a time-varying state variable, which is high-dimensional. We will first outline the model and present the probabilistic formulation of the equilibrium conditions. Section 2.2 will focus on the algorithm, and Section 2.3 will demonstrate the model's key equilibrium features through numerical results.

2.1 Model and Probabilistic Formulation

We will first consider the bond pricing in a secondary market, and then introduce the government's debt-maturity management problem with debt issuance costs.

2.1.1 Bond Pricing

Suppose the short rate r_t follows

$$\mathrm{d}r_t = \kappa(\theta - r_t)\, \mathrm{d}t + \sigma^r \sqrt{r_t} \mathrm{d}W_t, \tag{2}$$

where κ, θ, and σ^r are model parameters, and W_t represents one-dimensional standard Brownian motion. Consider a bond with maturity date T, a face value 1 and a coupon rate δ, with its price at time t for the short rate r_t given by $q(t, r_t)$, expressed as

$$q\left(t, r_t\right)=E_t\left[\delta \int_t^T e^{-\int_t^s r_u \mathrm{d}u} \mathrm{d}s+e^{-\int_t^T r_u \mathrm{d}u}\right]$$

To construct a martingale,

$$\delta \int_0^t e^{-\int_0^s r_u \mathrm{d}u} \mathrm{d}s+e^{-\int_0^t r_u \mathrm{d}u} q\left(t, r_t\right)=E_t\left[\delta \int_0^T e^{-\int_0^s r_u \mathrm{d}u} \mathrm{d}s+e^{-\int_0^T r_u \mathrm{d}u}\right].$$

The martingale representation theorem implies that there exists a predictable process σ_t^ψ such that[1]

$$\delta \int_0^t e^{-\int_0^s r_u \mathrm{d}u} \mathrm{d}s+e^{-\int_0^t r_u \mathrm{d}u} q\left(t, r_t\right)=q\left(0, r_0\right)+\int_0^t e^{-\int_0^s r_u \mathrm{d}u} \sigma_s^\psi \mathrm{d}W_s,$$

for an arbitrary $t<T$, and

$$\delta \int_0^T e^{-\int_0^s r_u \mathrm{d}u} \mathrm{d}s+e^{-\int_0^T r_u \mathrm{d}u} q\left(T, r_t\right)=q\left(0, r_0\right)+\int_0^T e^{-\int_0^s r_u \mathrm{d}u} \sigma_s^\psi \mathrm{d}W_s.$$

The difference of the two equations above yields

$$e^{-\int_0^t r_u \mathrm{d}u} q\left(t, r_t\right)=e^{-\int_0^T r_u \mathrm{d}u}+\delta \int_t^T e^{-\int_0^s r_u \mathrm{d}u} \mathrm{d}s-\int_t^T e^{-\int_0^s r_u \mathrm{d}u} \sigma_s^\psi \mathrm{d}W_s$$

Rewriting the integral equation in its differential form, we have

$$\begin{aligned}
\mathrm{d}\left(e^{-\int_0^t r_u \mathrm{d}u} q\left(t, r_t\right)\right) &= -\delta e^{-\int_0^t r_u \mathrm{d}u} \mathrm{d}t+e^{-\int_0^t r_u \mathrm{d}u} \sigma_t^\psi \mathrm{d}W_t \\
-r_t q\left(t, r_t\right) \mathrm{d}t+\mathrm{d}q\left(t, r_t\right) &= -\delta \mathrm{d}t+\sigma_t^\psi \mathrm{d}W_t.
\end{aligned}$$

Let $\psi\left(\tau, r\right)$ denote $q\left(T-\tau, r\right)$, then $\psi\left(T-t, r\right)=q\left(t, r\right)$ and the FBSDE with respect to the bond pricing is

$$\begin{aligned}
\mathrm{d}\psi(\tau, r_t) &= \left(r_t \psi(\tau, r_t)-\delta\right) \mathrm{d}t+\sigma_t^\psi \mathrm{d}W_t \\
\mathrm{d}\tau &= -\mathrm{d}t \\
\mathrm{d}r_t &= \kappa(\theta-r_t)\mathrm{d}t+\sigma^r \sqrt{r_t} \mathrm{d}W_t \\
\psi(0, r) &= 1
\end{aligned}$$

2.1.2 Maturity Management of a Government

The government maximizes the lifetime expected utility of its representative consumer, given an initial debt profile $f(t, \cdot)$ at calendar time t. The optimal control variable is the amount of debt the government issues at each maturity. Specifically, the government's dynamic optimization

[1] The term "predictable" means the realized value σ_t^ψ is fully determined given the information available right before time t.

problem is formulated as follows

$$V\left(r_t, f(t,\cdot)\right) = \max_{\iota(s,\cdot)} \; E_t\left[\int_t^\infty e^{-\rho s} U(c_s)\, ds\right] \tag{3}$$

subject to the constraints

$$c_t = y - f(t,0) + \int_0^T \left[q(t,r,\tau,\iota)\iota(t,\tau) - \delta f(t,\tau)\right] d\tau \tag{4}$$

$$\frac{\partial}{\partial t} f\left(t,\tau\right) = \iota(t,\tau) + \frac{\partial}{\partial \tau} f\left(t,\tau\right) \tag{5}$$

$$\mathrm{d}r_t = \kappa(\theta - r_t)\mathrm{d}t + \sigma^r \sqrt{r_t}\mathrm{d}W_t$$

where c_t denotes consumption, y is the government's constant income, and T represents the longest maturity at which the government issues debt. The variable $\iota(t,\cdot)$ indicates the issuance amount of debt at maturity τ. As the face value of the debt is 1, the government must repay $f(t,0)$. The bond price $q(t,r,\tau,\iota)$ at issuance is determined by

$$q(t,r,\tau,\iota) = \psi(\tau,r) - \frac{1}{2}\bar{\lambda}\psi(\tau,r)\iota(t,\tau),$$

where $\psi(\tau,r)$ is the price of debt with maturity τ in the secondary market, and $\bar{\lambda}\psi(\tau,r)$ reflects the cost of debt issuance. Readers are referred to Bigio et al. (2023) for the microfoundation of the issuance cost. Finally, Equation (5) describes the law of motion for the debt profile.

Dynamic Optimization. We focus on the Markov solution to the government's dynamic optimization problem with two state variables: the short rate r_t and the debt profile $f(t,\cdot)$. Dynamic programming is employed to derive the policy function, while the probabilistic formulation is used to determine the value function. The HJB equation is given by

$$\rho V(r, f(\cdot)) = \max_{\iota(\cdot)} \left\{U(c) + \int_0^T \frac{\partial V}{\partial f(\tau)}\left(\iota(\tau) + \frac{\partial}{\partial \tau} f(t,\tau)\right) \mathrm{d}\tau\right\} + \kappa(\theta - r)\frac{\partial V}{\partial r} + (\sigma^r)^2 r \frac{\partial^2 V}{\partial r^2}$$

$$c = y - f(0) + \int_0^T \left[q(r,\tau,\iota)\iota(\tau) - \delta f(t,\tau)\right] d\tau$$

$$q(r,\tau,\iota) = \psi(\tau,r) - \frac{1}{2}\bar{\lambda}\psi(\tau,r)\iota(\tau)$$

The first-order condition with respect to $\iota(\tau)$ is

$$U'(c)\left(\psi(\tau,r) - \bar{\lambda}\psi(\tau,r)\iota\right) + \frac{\partial V}{\partial f(\tau)} \leq 0 \text{ with equality if } \iota > 0. \tag{6}$$

Given the state variables r and $f(\tau)$, as well as the value function $V(r, f(\cdot))$ and the bond pricing function $\psi(r,\tau)$, the FOC above and the budget constraint (4) jointly determine the debt issuance policy $\iota(\tau, r, f(\cdot))$ and the consumption policy $c(r, f(\cdot))$.

Given the policy function, we resort to the probabilistic formulation to define the value function $V(r, f(\cdot))$. Based on the budget constraint (4), the policy function $\iota(r_t, f(t,\cdot))$ defines the consumption stream c_t, which, in turn, determines the lifetime expected utility (3). We

define a martingale as follows

$$\int_0^t e^{-\rho s} U\left(c_s\right) \mathrm{d}s + e^{-\rho t} V\left(r_t, f\left(t, \cdot\right)\right) = E_t\left[\int_0^\infty e^{-\rho s} U\left(c_s\right) \mathrm{d}s\right]$$

assuming the transversality condition is satisfied. The martingale representation theorem implies that there exists a predictable process σ_t^V such that

$$\int_0^t e^{-\rho s} U\left(c_s\right) \mathrm{d}s + e^{-\rho t} V\left(r_t, f\left(t, \cdot\right)\right) = V\left(r_0, f\left(0, \cdot\right)\right) + \int_0^t \sigma_s^V \mathrm{d}W_s$$

for an arbitrary t. The differential form of the above integral equation yields the BSDE with respect to $V\left(r_t, f\left(t, \cdot\right)\right)$. Including the law of motion for the backward-looking processes r_t and $f\left(t, \cdot\right)$, we obtain the FBSDE system defining the value function $V\left(r, f\left(\cdot\right)\right)$

$$\begin{aligned}
\mathrm{d}V_t &= \left(\rho V_t - U\left(c_t\right)\right) \mathrm{d}t + \sigma_t^V \mathrm{d}W_t \\
\mathrm{d}f\left(t, \tau\right) &= \left(\iota\left(t, \tau\right) + \frac{\partial}{\partial \tau} f\left(t, \tau\right)\right) \mathrm{d}t \\
\mathrm{d}r_t &= \kappa\left(\theta - r_t\right) \mathrm{d}t + \sigma^r \sqrt{r_t} \mathrm{d}W_t.
\end{aligned}$$

2.2 Numerical Methods

This section will focus on the numerical method for solving the government's debt-maturity management problem. The numerical method used for solving bond pricing in the secondary market is standard and has been relegated to the Appendix.

2.2.1 Finite Volume Method

$f(\tau)$ is an infinite-dimensional object, and $V(r, f(\cdot))$ is a functional of $f(\tau)$. We employ the finite volume method to approximate the value function, the law of motion for the debt profile (5), and the first-order condition (6). Specifically, we divide the interval $[0, T]$, which represents the range of the debt's time-to-maturity, into K subintervals such that $0 = x_0 < x_1 < \cdots < x_K = T$. The debt profile $f(t, \tau)$ is then approximated using K scalars

$$f_t^k = \frac{1}{x_k - x_{k-1}} \int_{x_{k-1}}^{x_k} f(t, \tau) \mathrm{d}\tau.$$

Here, f_t^k can be interpreted as the average outstanding debt with a time-to-maturity within $[x_{k-1}, x_k]$.[2] In other words, the debt profile is approximated by a step function

$$\sum_{k=1}^{K} f_t^k \mathbf{1}\left\{\tau^{k-1} \leq \tau < \tau^k\right\}.$$

Similar to the debt profile, we approximate the policy function $\iota(t, \tau)$ with K scalars ι_t^k such

[2] A technical assumption is made that there is no mass at any boundary point x_k.

that

$$U'(c_t)\left(\psi(\hat{x}^k, r) - \bar{\lambda}\psi(\hat{x}^k, r)\iota_t^k\right) + \frac{\partial V}{\partial f_t^k} \leq 0 \text{ with equality if } \iota_t^k > 0,$$

where $\hat{x}^k$ is the midpoint of the interval $[x^{k-1}, x^k]$. ι_t^k is interpreted as the average issuance rate of new debt maturing within $[x^{k-1}, x^k]$. Given this specification of ι_t^k, the volume of outstanding debt within $[x_t^{k-1}, x_t^k]$ increases by $\iota_t^k\left(x^k - x^{k-1}\right)\mathrm{d}t$ due to new issuance, increases by $f_t^{k+1}\mathrm{d}t$, and decreases by $f_t^k\mathrm{d}t$ due to the aging of outstanding debt. Overall, the law of motion for f_t^k is

$$\mathrm{d}f_t^k = \left(\iota_t^k + \frac{f_t^{k+1} - f_t^k}{x_k - x_{k-1}}\right)\mathrm{d}t.$$

Hereafter, f_t denotes the vector $[f_t^1, \cdots, f_t^K]$.

2.2.2 Numerical Scheme

We use feedforward neural networks to approximate the value function, denoted as $\hat{V}(\cdot;\Theta)$, and the consumption policy function $\hat{c}(\cdot;\Theta)$. The debt issuance policy function is recovered based on the FOC (6).

Initialization. We discretize time interval $[0, t_{\mathbf{I}}]$ evenly into $\mathbf{I}$ subintervals: $0 = t_0 < t_1 < t_2 < \cdots < t_{\mathbf{I}}$. Then, We simulate M sample paths of Brownian motions $\{W_{i,m}\}_{i=0,m=1}^{\mathbf{I}-1,M}$ and initial states $\{r_{0,m}, f_{0,m}\}_{m=1}^{M}$. Here, We drop the subscript m to simplify notation. Let $\Delta \equiv t_{i+1} - t_i$ and $w_i \equiv W_{i+1} - W_i$. Initialize $V_0 = \hat{V}\left(x_0, f_0; \Theta\right)$ and $c_0 = \hat{c}\left(x_0, f_0; \Theta\right)$. Next, we will repeat the following procedure for i ranging from 0 to $\mathbf{I} - 1$.

Computation Steps

1. Use a pretrained neural network for bond pricing to produce $\hat{\psi}_i^k = \psi(\hat{x}^k, r_i; \Theta)$ the price of debt at maturity $\hat{x}^k$. Use the neural network to produce $\sigma_i^V = \sigma^V(r_i, f_i; \Theta)$, $\hat{c}_i = c(r_i, f_i; \Theta)$, and the partial derivatives $\frac{\partial}{\partial f_i^k}\hat{V}(r_i, f_i; \Theta)$. Then, calculate bond issuance at $\hat{x}^k$ using

$$\iota_i^k = \max\left\{\frac{1}{\bar{\lambda}}\frac{\hat{\psi}_i^k + \frac{\partial \hat{V}_i/\partial f_i^k}{U'(\hat{c}_i)}}{\hat{\psi}_i^k}, 0\right\},$$

   which is based on the the first-order condition (6).

2. Calculate the price of bonds at which the government issued at the primary market:

$$q_i^k = \hat{\psi}_i^k - \frac{1}{2}\bar{\lambda}\hat{\psi}_i^k\iota_i^k$$

   and the consumption based on the budget constraint:

$$c_i = I_t - f_i^1 + \sum_{k=2}^{K}\left[(q_i^k\iota_i^k - \delta f_i^k)(x_k - x_{k-1})\right]$$

3. Construct the loss for c:

$$\text{Loss}_{c,i} = (c_i - \hat{c}_i)^2$$

4. Update the BSDE and SDEs:

$$\begin{aligned} V_{i+1} &= V_i + (\rho V_i - U(\hat{c}))\Delta + \sigma_i^V (W_{i+1} - W_i) \\ r_{i+1} &= r_i + \kappa(\theta - r_i)\Delta + \sigma^r \sqrt{r_i}(W_{i+1} - W_i) \\ f_{i+1}^k &= f_i^k + \left(\iota_i^k + \frac{f_i^{k+1} - f_i^k}{x_k - x_{k-1}} \right) \Delta \end{aligned}$$

5. Use a neural network to produce $\hat{V}_{i+1} = V(r_{i+1}, f_{i+1}; \Theta)$, and construct the loss for the value function:

$$\text{Loss}_{v,i} = (V_{i+1} - \hat{V}_{i+1})^2$$

6. Keep track of the loss:

$$\text{Loss} = \text{Loss} + \frac{1}{MN} \sum_{i=1}^{N} (\text{Loss}_{c,i} + \text{Loss}_{v,i})$$

7. Repeat steps 1 to 6 until all **I** time iterations are finished.

2.3 Numerical Results

2.3.1 Value Function and Debt Profile Dynamics

Figure 1 illustrates the value function V as a function of the short-term interest rate r under different debt profiles. The top panel shows V versus r under three debt profiles: debt outstanding 1 (blue), debt outstanding 2 (orange), and debt outstanding 3 (green). The bottom panel displays the three debt profiles — the outstanding debt as a function of maturity τ (in years), with each point on the debt profile lines representing the midpoint of the discretized τ intervals used in the numerical computation.

The top panel shows that the value function V decreases as the short-term interest rate r rises, with all three lines sloping downward. This reflects the negative effect of higher interest rates on the government's value function. Higher interest rates lower the price of government-issued bonds, reducing the proceeds from debt issuance, as expected.

The average maturity of the debt profile also affects the value function. Debt outstanding 1 (blue) has the shortest average maturity, followed by debt outstanding 2 (orange) and debt outstanding 3 (green). Consequently, V is highest for debt outstanding 1 and lowest for debt outstanding 3, indicating that a longer average maturity leads to a lower value function. Intuitively, this occurs because longer maturities increase the debt burden through coupon payments.

The bottom panel highlights the discretization of the maturity τ. Each point on the debt profile lines marks the midpoint of the discretized τ intervals, illustrating how debt is distributed across maturities for each profile.

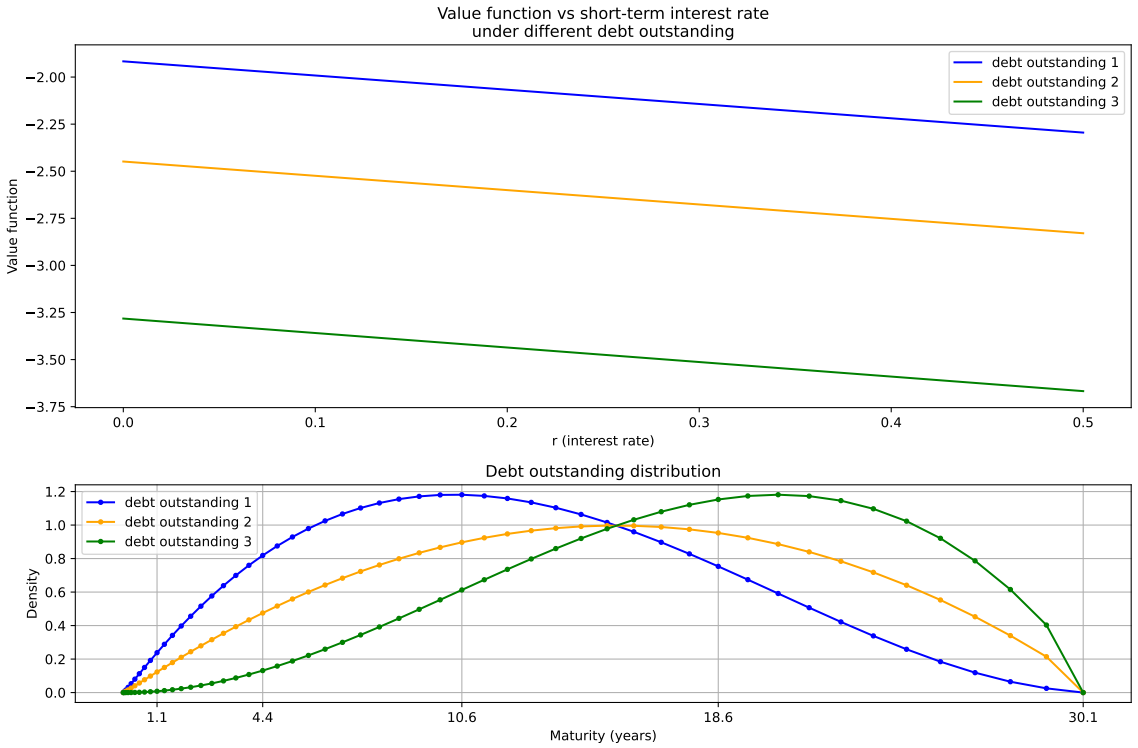

Figure 1: Value function
The upper panel shows the continuation value V as a function of short-term interest rate r under different debt profiles, and the lower panel presents the corresponding debt outstanding distributions.

2.3.2 Consumption and Debt Profile Dynamics

Figure 2 illustrates the consumption of the representative agent c as a function of the short-term interest rate r under different debt profiles. The top panel shows c versus r for three debt profiles: debt outstanding 1 (blue), debt outstanding 2 (orange), and debt outstanding 3 (green). The bottom panel displays the three debt profiles, consistent with Figure 1.

The top panel of Figure 2 shows that consumption c decreases as the short-term interest rate r rises, with all three lines sloping downward. This stems from reduced income from bond issuance.Higher interest rates lower the price of bonds to be issued and, as shown in Figure 3, reduce debt issuance. The average maturity of the debt profile also impacts consumption. Debt outstanding 1 has the shortest average maturity, followed by debt outstanding 2, and debt outstanding 3 with the longest average maturity. Consequently, c is highest for debt outstanding 1 and lowest for debt outstanding 3, indicating that a longer average maturity leads to lower consumption-—an effect akin to its impact on the value function.

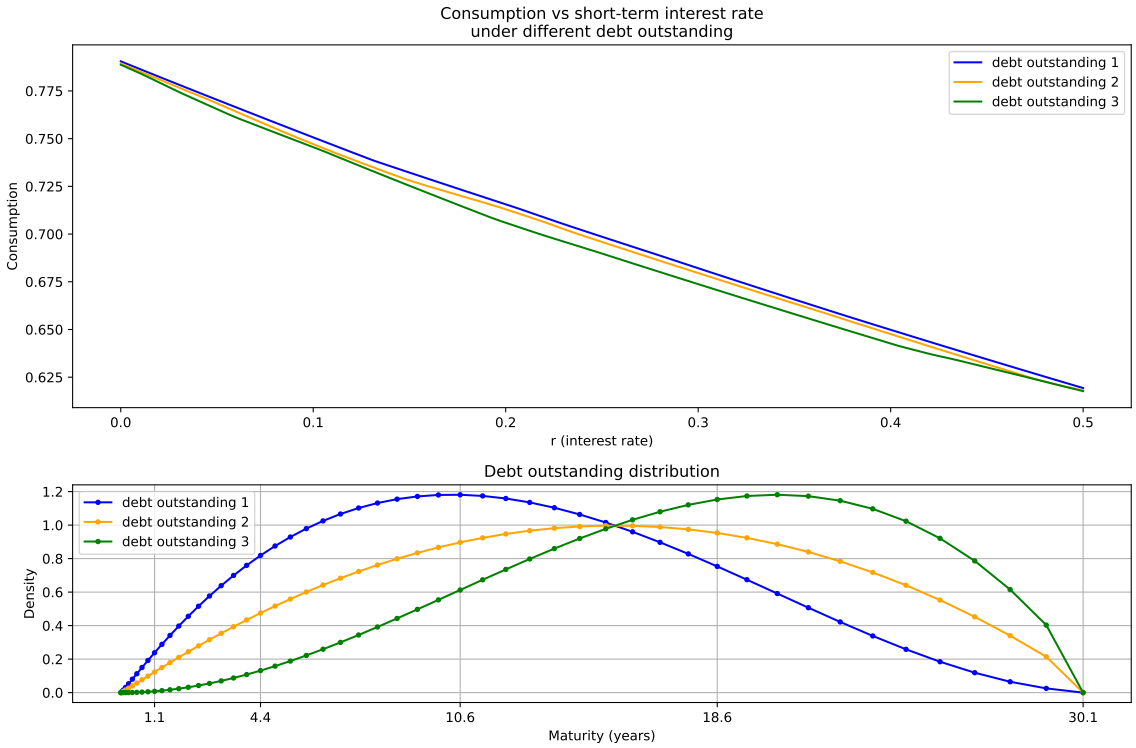

Figure 2: Consumption
The top panel shows c for debt outstanding 1 (blue), debt outstanding 2 (orange), and debt outstanding 3 (green) as r varies from 0.0 to 0.5. The bottom panel shows the density of debt outstanding for each profile across maturities τ, with points marking the midpoints of the discretized τ intervals.

2.3.3 Debt Issuance Across Maturities

Figure 3 illustrates the debt issuance at maturities $\tau = 0.9$ years and $\tau = 28.9$ years as a function of the short-term interest rate r under two debt profiles. These maturities represent short- and long-term issuance, respectively. The top two panels show issuance for $\tau = 0.9$ years (left) and $\tau = 28.9$ years (right) for debt outstanding 1 (blue) and debt outstanding 2 (red) as r varies from 0.0 to 0.5. The bottom panel shows the two debt profiles, consistent with Figure 1.

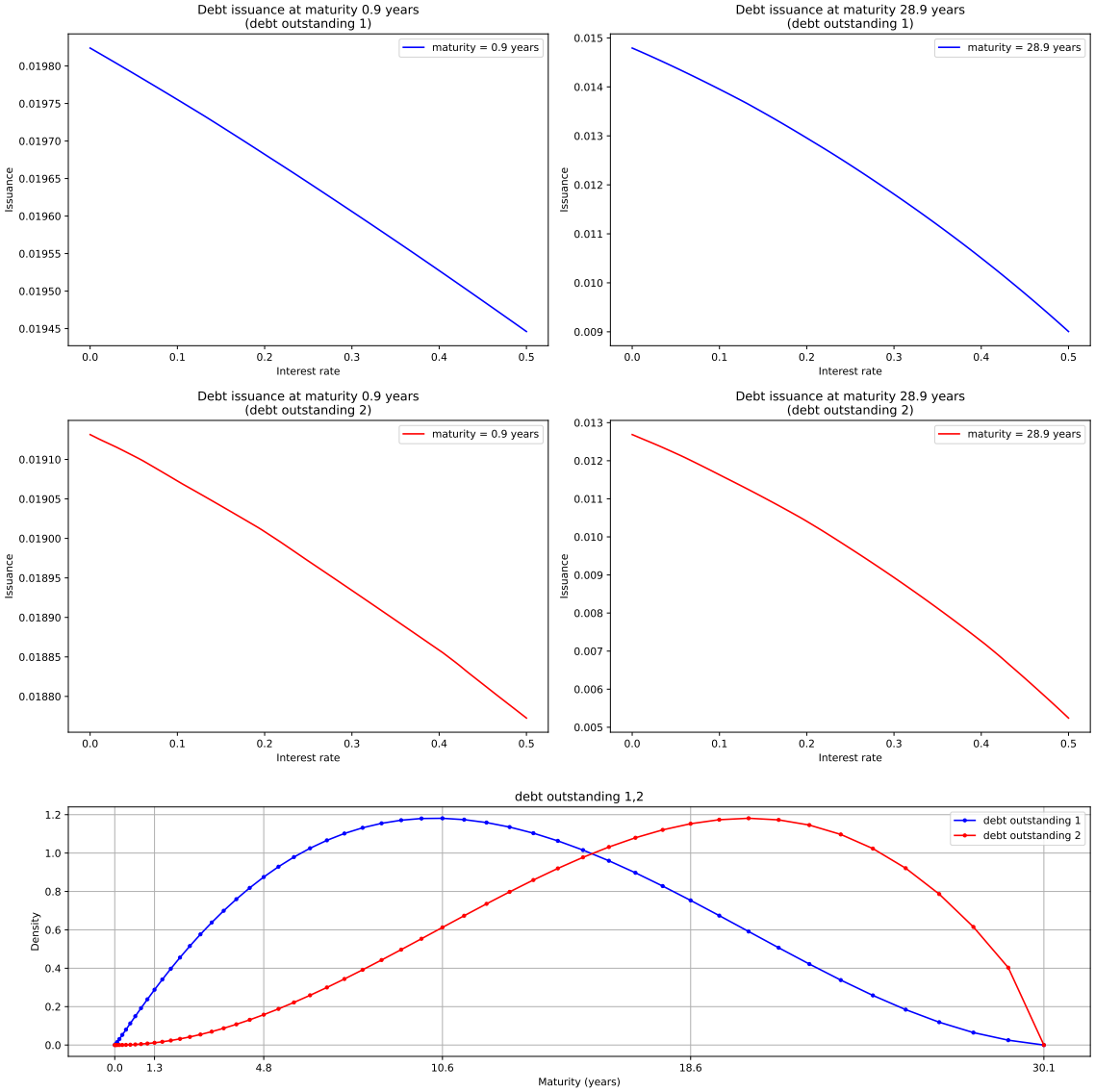

Figure 3: Debt issuance against interest rate
The upper four panels show issuance for debt outstanding 1 (blue) and debt outstanding 2 (red) as r varies from 0.0 to 0.5 at different maturities ($\tau = 0.9$ in left panels and $\tau = 28.9$ in the right panels). The bottom panel shows the density of debt outstanding for each profile across maturities τ, with points marking the midpoints of the discretized τ intervals.

Debt issuance at both short ($\tau = 0.9$ years) and long ($\tau = 28.9$ years) maturities decreases as the short-term interest rate r rises, regardless of the debt profile. This is straightforward because higher rates reduce the proceeds of debt issuance, with the coupon and principal held constant.

Issuance for debt outstanding 1 (blue) exceeds that for debt outstanding 2 (red) at both maturities across all interest rates, reflecting differences in the debt profiles. This aligns with our earlier finding that a shorter average duration of outstanding debt enables the government to issue more.

2.3.4 Debt Issuance Distribution Across Maturities

Figure 4 illustrates the debt issuance across various maturities under different short-term interest rates r and debt profiles. The top four panels show histograms of debt issuance for $r = 0.0\%$ (left) and $r = 5.1\%$ (right) for debt outstanding 1 (blue) and debt outstanding 2 (red). The bottom panel shows the two debt profiles, consistent with Figure 1.

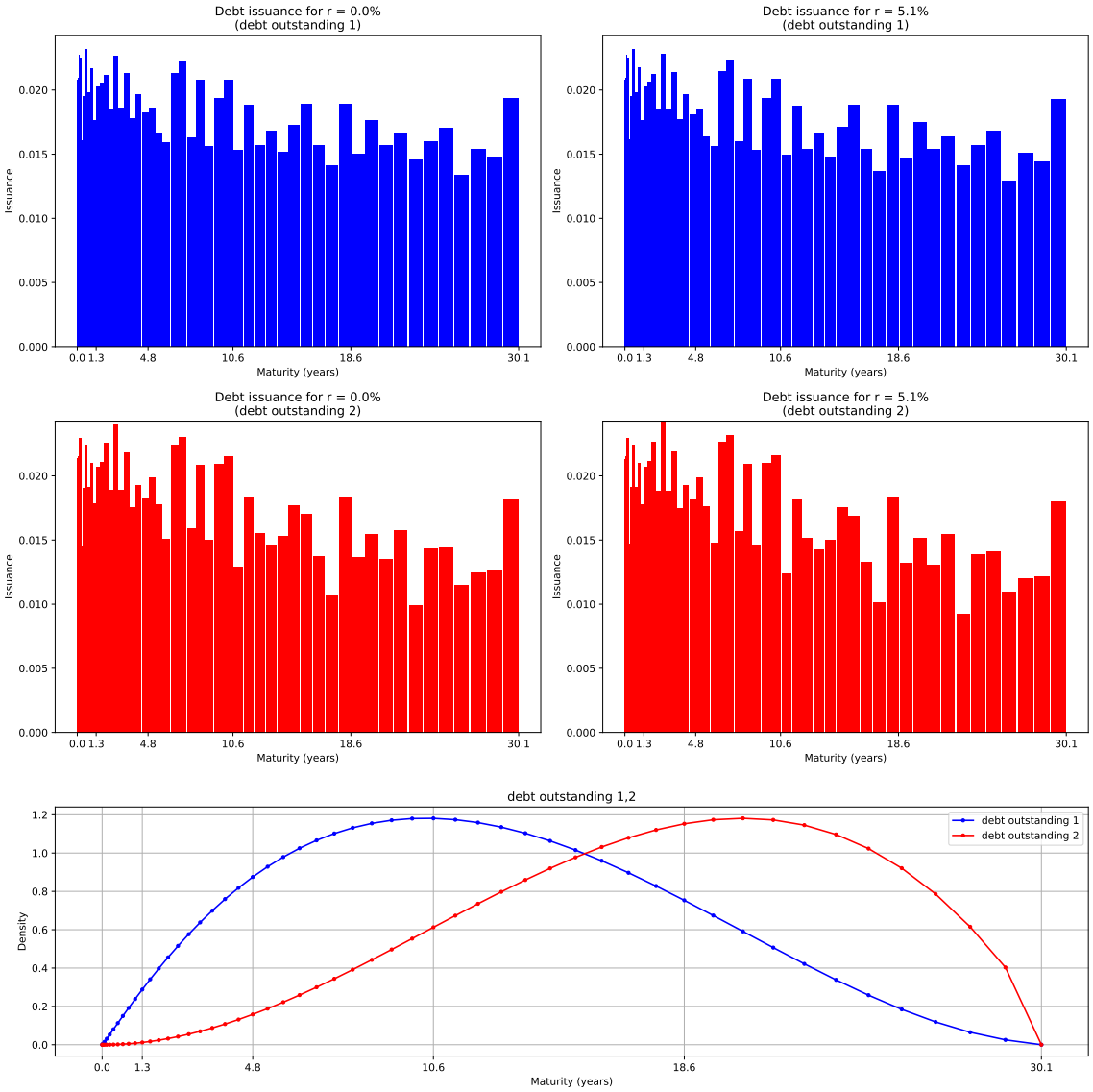

Figure 4: Debt issuance over maturity
The top panels show histograms of debt issuance for $r = 0.0\%$ (left) and $r = 5.1\%$ (right) for debt outstanding 1 (blue) and debt outstanding 2 (red). The bottom panel shows the density of debt outstanding for each profile across maturities τ, with points marking the midpoints of the discretized τ intervals.

3 Preferred Habitat Model with Intermediary Asset Pricing

We analyze a preferred habitat model of the term structure of interest rates proposed by Kekre, Lenel and Mainardi (2024), which considers two types of agents: preferred habitat investors and arbitrageurs. In Kekre et al. (2024), the arbitrageurs' discount rate is assumed to be arbitrarily large to simplify the model by suppressing intertemporal hedging motives. Here, we examine

a more general case with a finite discount rate, which is computationally more challenging due to the inclusion of an additional forward-looking variable that captures future investment opportunities.

3.1 Model

The short rate r_t is exogenous and follows an Ornstein-Uhlenbeck process

$$\mathrm{d}r_t = \kappa_r(\bar{r} - r_t)\,\mathrm{d}t + \sigma_r\,\mathrm{d}B_{r,t} \tag{7}$$

where κ_r denotes the mean-reversion rate, $\bar{r}$ represents the long-term mean of the short rate, σ_r is the volatility, and $B_{r,t}$ is a one-dimensional standard Brownian motion. At any time t, there exists a continuum of zero-coupon bonds with maturities $\tau \in (0, \infty)$. The price of a bond with maturity τ is denoted by P_t^τ, with a face value of 1.

The aggregate positions of debt with maturity τ held by preferred-habitat investors are given by

$$Z_t^\tau = -\alpha(\tau)\log(P_t^\tau) - \theta_0(\tau) - \theta_1(\tau)\beta_t$$

where β_t is a state variable that captures the stochastic changes in investors' preferences. Note that β_t drives the demand for debt across different maturities. The law of motion for β_t is

$$d\beta_t = -\kappa_\beta\beta_t\,\mathrm{d}t + \sigma_\beta\,\mathrm{d}B_{\beta,t}, \tag{8}$$

where κ_β and σ_β are parameters, and $B_{\beta,t}$ is a one-dimensional standard Brownian motion independent of $B_{r,t}$. For specific numerical results presented later, and following Kekre et al. (2024), we assume that

$$\alpha(\tau) = \alpha e^{-\tau}, \quad \theta_0(\tau) = \theta_0 e^{-\tau}, \quad \theta_1(\tau) = \theta_1 e^{-\tau}$$

if $\tau \leq 30$, and $\alpha(\tau) = \theta_0(\tau) = \theta_1(\tau) = 0$ if $\tau > 30$.

$B_{r,t}$ and $B_{\beta,t}$ are the only two exogenous shocks in the model. Consequently, we postulate that the bond price P_t^τ follows a BSDE

$$\frac{\mathrm{d}P_t^\tau}{P_t^\tau} = \omega_t^\tau \mathrm{d}t + \eta_{r,t}^\tau \mathrm{d}B_{r,t} + \eta_{\beta,t}^\tau \mathrm{d}B_{\beta,t}, \tag{9}$$

where ω_t^τ is to be determined later, and $\eta_{r,t}^\tau$ and $\eta_{\beta,t}^\tau$ are the solutions of the BSDE.

Arbitrageurs. Arbitrageurs trade debt instruments of all maturities. They are born and die at a rate of ξ, discount future utility at a rate of ρ, and have CRRA preferences over their wealth w_t upon death, with a risk aversion parameter γ. They do not consume before death and are endowed with an initial wealth $\bar{W}$ at birth. An arbitrageur maximizes their lifetime expected utility by selecting a portfolio of debt across various maturities

$$V_t = \max_{\{x_{t+s}^\tau\}^\tau} E_t\left[\int_0^\infty e^{-(\xi+\rho)s}(\xi+\rho)\left(\frac{w_{t+s}^{1-\gamma}-1}{1-\gamma}\right)\mathrm{d}s\right]$$

subject to the law of motion for the individual wealth w_t

$$\mathrm{d}w_t = w_t r_t \mathrm{d}t + \int_0^\infty x_t^\tau \left(\frac{\mathrm{d}P_t^\tau}{P_t^\tau} - r_t \mathrm{d}t \right) \mathrm{d}\tau,$$

where x_t^τ represents the arbitrageur's position in debt with maturity τ.

Aggregate States. Let X_t^τ denote the arbitrageurs' aggregate demand for the debt. The market-clearing condition

$$Z_t^\tau + X_t^\tau = 0 \quad \text{for each } \tau \in (0, \infty) \text{ and each } t$$

implies the equilibrium demand for bonds

$$X_t^\tau = \alpha(\tau) \log(P_t^\tau) + \theta_0(\tau) + \theta_1(\tau)\beta_t \tag{10}$$

Hence, the law of motion for the aggregate arbitrageur wealth, W_t, is given by

$$\begin{aligned} \mathrm{d}W_t &= W_t r_t \mathrm{d}t + \int_0^\infty X_t^\tau \left(\frac{\mathrm{d}P_t^\tau}{P_t^\tau} - r_t \mathrm{d}t \right) \mathrm{d}\tau + \xi(\bar{W} - W_t)\mathrm{d}t \\ &= \omega_t \mathrm{d}t + \eta_{r,t} \mathrm{d}B_{r,t} + \eta_{\beta,t} \mathrm{d}B_{\beta,t}, \text{ where} \\ \omega_t &\equiv W_t r_t + \xi(\bar{W} - W_t) + \int_0^\infty X_t^s (\omega_t^s - r_t) \mathrm{d}s \\ \eta_{r,t} &\equiv \int_0^\infty X_t^s \eta_{r,t}^s \mathrm{d}s, \qquad \eta_{\beta,t} \equiv \int_0^\infty X_t^s \eta_{\beta,t}^s \mathrm{d}s. \end{aligned} \tag{11}$$

The aggregate states of the economy are r_t, β_t, and W_t.

3.1.1 Probabilistic Formulation

Given the BSDE for P_t^τ, we rewrite the law of motion for an arbitrageur

$$\frac{\mathrm{d}w_t}{w_t} = \left(r_t + \int_0^\infty \hat{x}_t^\tau \left(\omega_t^\tau - r_t \mathrm{d}t \right) \mathrm{d}\tau \right) \mathrm{d}t + \left(\int_0^\infty \hat{x}_t^\tau \eta_{r,t}^\tau \mathrm{d}s \right) \mathrm{d}B_{r,t} + \left(\int_0^\infty \hat{x}_t^\tau \eta_{\beta,t}^\tau \mathrm{d}s \right) \mathrm{d}B_{\beta,t}, \tag{12}$$

where $\hat{x}_t^\tau \equiv \frac{x_t^\tau}{w_t}$. Given the optimal portfolio $\{\hat{x}_t^\tau, 0 \leq \tau < \infty\}$, consider the construction of a martingale

$$\int_0^t e^{-(\xi+\rho)s} (\xi + \rho) \left(\frac{w_s^{1-\gamma} - 1}{1-\gamma} \right) \mathrm{d}s + e^{-(\xi+\rho)t} V_t = E_t \left[\int_0^\infty e^{-(\xi+\rho)s} (\xi + \rho) \left(\frac{w_s^{1-\gamma} - 1}{1-\gamma} \right) \mathrm{d}s \right].$$

By the martingale representation theorem, there exist predictable stochastic processes $\sigma_{r,t}^V$ and $\sigma_{\beta,t}^V$ such that

$$\int_0^t e^{-(\xi+\rho)s} (\xi + \rho) \left(\frac{w_s^{1-\gamma} - 1}{1-\gamma} \right) \mathrm{d}s + e^{-(\xi+\rho)t} V_t = V_0 + \int_0^t e^{-(\xi+\rho)s} \sigma_{r,s}^V \mathrm{d}B_{r,s} + \int_0^t e^{-(\xi+\rho)s} \sigma_{\beta,s}^V \mathrm{d}B_{\beta,s}$$

The differential form of the above integral equation can be written as

$$\mathrm{d}V_t = -\left(\xi+\rho\right)\left(\frac{w_t^{1-\gamma}-1}{1-\gamma}-V_t\right)\mathrm{d}t+\sigma_{r,t}^V\mathrm{d}B_{r,t}+\sigma_{\beta,t}^V\mathrm{d}B_{\beta,t}$$

Given the linearity of the dynamic budget constraint (12) and the homogeneity of the utility function, we conjecture that

$$V_t=\frac{\left(\nu_t w_t\right)^{1-\gamma}-1}{1-\gamma},$$

where ν_t satisfies the BSDE

$$\frac{\mathrm{d}\nu_t}{\nu_t}=\omega_t^\nu\mathrm{d}t+\eta_{r,t}^\nu\mathrm{d}B_{r,t}+\eta_{\beta,t}^\nu\mathrm{d}B_{\beta,t}. \tag{13}$$

ν_t is interpreted as the arbitrageur's wealth multiplier, which reflects future investment opportunities. Applying Ito's formula to V_t yields

$$\begin{aligned}\mathrm{d}V_t=&\nu_t^{1-\gamma}w_t^{1-\gamma}\left(\left(r_t+\int_0^\infty\hat{x}_t^\tau\left(\omega_t^\tau-r_t\mathrm{d}t\right)\mathrm{d}\tau\right)\mathrm{d}t+\left(\int_0^\infty\hat{x}_t^\tau\eta_{r,t}^\tau\mathrm{d}s\right)\mathrm{d}B_{r,t}+\left(\int_0^\infty\hat{x}_t^\tau\eta_{\beta,t}^\tau\mathrm{d}s\right)\mathrm{d}B_{\beta,t}\right)\\&+\nu_t^{1-\gamma}w_t^{1-\gamma}\left(\omega_t^\nu\mathrm{d}t+\eta_{r,t}^\nu\mathrm{d}B_{r,t}+\eta_{\beta,t}^\nu\mathrm{d}B_{\beta,t}\right)-\frac{1}{2}\gamma\nu_t^{1-\gamma}w_t^{1-\gamma}\left(\left(\int_0^\infty\hat{x}_t^\tau\eta_{r,t}^\tau\mathrm{d}s\right)^2+\left(\int_0^\infty\hat{x}_t^\tau\eta_{\beta,t}^\tau\mathrm{d}s\right)^2\right)\mathrm{d}t\\&-\frac{1}{2}\gamma\nu_t^{1-\gamma}w_t^{1-\gamma}\left(\left(\eta_{r,t}^\nu\right)^2+\left(\eta_{\beta,t}^\nu\right)^2\right)\mathrm{d}t+\left(1-\gamma\right)\nu_t^{1-\gamma}w_t^{1-\gamma}\left(\eta_{r,t}^\nu\int_0^\infty\hat{x}_t^\tau\eta_{r,t}^\tau\mathrm{d}s+\eta_{\beta,t}^\nu\int_0^\infty\hat{x}_t^\tau\eta_{\beta,t}^\tau\mathrm{d}s\right)\mathrm{d}t\end{aligned}$$

The drift terms of $\mathrm{d}V_t$ in the two equations above must be identical. Hence,

$$\begin{aligned}-\left(\xi+\rho\right)\left(\frac{\nu_t^{-(1-\gamma)}-1}{1-\gamma}\right)=&\,r_t+\int_0^\infty\hat{x}_t^\tau\left(\omega_t^\tau-r_t\mathrm{d}t\right)\mathrm{d}\tau+\omega_t^\nu+\left(1-\gamma\right)\left(\eta_{r,t}^\nu\int_0^\infty\hat{x}_t^\tau\eta_{r,t}^\tau\mathrm{d}s+\eta_{\beta,t}^\nu\int_0^\infty\hat{x}_t^\tau\eta_{\beta,t}^\tau\mathrm{d}s\right)\\&-\frac{1}{2}\gamma\left(\left(\int_0^\infty\hat{x}_t^\tau\eta_{r,t}^\tau\mathrm{d}s\right)^2+\left(\int_0^\infty\hat{x}_t^\tau\eta_{\beta,t}^\tau\mathrm{d}s\right)^2+\left(\eta_{r,t}^\nu\right)^2+\left(\eta_{\beta,t}^\nu\right)^2\right).\end{aligned}$$

If $\{\hat{x}_t^\tau,\tau\geq 0\}$ is chosen to maximize the right-hand side of the equation above, then the equation is an HJB equation, which gives rise to the drift term of BSDE (13). The FOC of the HJB equation above w.r.t. $\hat{x}_t^\tau$ is

$$\omega_t^\tau-r_t=\gamma\left(\eta_{r,t}^\tau\left(\int_0^\infty\hat{x}_t^s\eta_{r,t}^s\mathrm{d}s\right)+\eta_{\beta,t}^\tau\left(\int_0^\infty\hat{x}_t^s\eta_{\beta,t}^s\mathrm{d}s\right)\right)-\left(1-\gamma\right)\left(\eta_{r,t}^\tau\eta_{r,t}^\nu+\eta_{\beta,t}^\tau\eta_{\beta,t}^\nu\right), \tag{14}$$

which gives rise to the drift term of BSDE (9). Now, we verify that the law of motion for ν_t is independent of the arbitrageur's individual wealth level w_t, which confirms our conjecture regarding V_t. Moreover, arbitrageurs' portfolio choice is linear in their wealth levels. Hence

$$\hat{x}_t^\tau=\frac{X_t^\tau}{W_t},$$

that is, an individual arbitrageur's portfolio weight on debt at maturity τ is equal to the ratio of the aggregate demand for debt of maturity τ to the total wealth of the arbitrageur sector.

In summary, the solution to the model is defined by a coupled FBSDE system, which consists

of the forward SDEs (7), (8), and (11), and the backward SDEs (9) for each maturity τ and (13) for ν_t.

When solving for $P^\tau(\cdot)$ and $\nu(\cdot)$ as functions of the state variables r_t, β_t, and W_t, it is more convenient to approximate $\log(P^\tau(\cdot))$ and $\log(\nu(\cdot))$, as these logarithmic forms can take values over a wider range. Thus, we derive BSDEs for $\log(P_t^\tau)$ and $\log(\nu_t)$ using Ito's formula

$$d\log P_t^\tau = \left(\omega_t^\tau - \frac{1}{2}(\eta_{r,t}^\tau)^2 - \frac{1}{2}(\eta_{\beta,t}^\tau)^2\right) dt + \eta_{r,t}^\tau\, dB_{r,t} + \eta_{\beta,t}^\tau\, dB_{\beta,t}$$

$$d\log \nu_t = \left(\omega_t^\nu - \frac{1}{2}(\eta_{r,t}^\nu)^2 - \frac{1}{2}(\eta_{\beta,t}^\nu)^2\right) dt + \eta_{r,t}^\nu\, dB_{r,t} + \eta_{\beta,t}^\nu\, dB_{\beta,t}$$

3.2 Numerical Methods

3.2.1 Finite Volume Method

The integration in first-order condition (14) involves a high-dimensional object $\hat{x}_t^\tau$ at time t. We employ the finite volume method to numerically implement this first-order condition. As described in Section 2, we partition $[0,\infty)$—the interval where the time-to-maturity of debt lies—into K sub-intervals such that $0 = \tau_0 < \tau_1 < \cdots < \tau_K = T$. The aggregate demand for debt X_t^τ is approximated using K scalars

$$X_t^k = \frac{1}{\tau_k - \tau_{k-1}} \int_{\tau_{k-1}}^{\tau_k} X_t^\tau \mathrm{d}\tau.$$

The functional specification of aggregate demand (10) ensures that X_t^τ is arbitrarily small for $\tau > T$. Furthermore, X_t^k is determined by the aggregate demand function at the midpoint of the corresponding interval

$$X_t^k = \alpha(\hat{\tau}^k)\log(P_t^{\hat{\tau}^k}) + \theta_0(\hat{\tau}^k) + \theta_1(\hat{\tau}^k)\beta_t, \text{ where } \hat{\tau}^k = \frac{1}{2}(\tau^{k-1} + \tau^k).$$

Given the discretization outlined above, the finite volume approximation of FOC (14) is

$$\begin{aligned}\omega_t^\tau - r_t = \gamma &\left(\eta_{r,t}^\tau \left(\sum_{k=1}^{K} \hat{x}_t^k \eta_{r,t}^k (\tau^k - \tau^{k-1})\right) + \eta_{\beta,t}^\tau \left(\sum_{k=0}^{K} \hat{x}_t^k \eta_{\beta,t}^k (\tau^k - \tau^{k-1})\right)\right) \\ &- (1-\gamma)\left(\eta_{r,t}^k \eta_{r,t}^\nu + \eta_{\beta,t}^k \eta_{\beta,t}^\nu\right),\end{aligned} \tag{15}$$

where $\omega_t^k, \eta_{r,t}^k$, and $\eta_{\beta,t}^k$ refer to $\omega_t^\tau, \eta_{r,t}^\tau$, and $\eta_{\beta,t}^\tau$ evaluated at the midpoint of the interval $[\tau^{k-1}, \tau^k]$, i.e., $\tau = 0.5(\tau^{k-1} + \tau^k)$.

3.2.2 Numerical Scheme

We use feedforward neural networks to approximate the bond pricing function, $\hat{P}(\tau, r, \beta, W; \Theta)$, the wealth multiplier $\hat{v}(r, \beta, W; \Theta)$, and also their volatility terms.

Initialization. We discretize time interval $[0, t_{\mathbf{I}}]$ evenly into $\mathbf{I}$ subintervals: $0 = t_0 < t_1 < t_2 < \cdots < t_{\mathbf{I}}$. Simulate M sample paths of Brownian motions for β and r: $\{B_{\beta,i,m}, B_{r,i,m}\}_{i=0,m=1}^{I-1,M}$,

where m denotes each sample path. The path subscript m will be dropped later. The length of a time interval is Δ. Initialize state variables $(W_0, r_0, \beta_0, \tau_0)$. Use a neural network to initialize $\log P_0 = \log \hat{P}(\tau_0, W_0, r_0, \beta_0)$ and $\log \nu_0 = \log \hat{\nu}(W_0, r_0, \beta_0)$. Set loss $= 0$.

1. Use the neural network to output $\log P_i^k = \log \hat{P}(\hat{\tau}^k, W_i, r_i, \beta_i), \eta_{r,i}^k = \eta_r(\hat{\tau}^k, W_i, r_i, \beta_i), \eta_{\beta,i}^k = \eta_\beta(\hat{\tau}^k, W_i, r_i, \beta_i)$;
2. Calculate the demand for bonds at each maturity: $X_i^k = \alpha(\hat{\tau}^k)\log(P_t^{\hat{\tau}^k}) + \theta_0(\hat{\tau}^k) + \theta_1(\hat{\tau}^k)\beta_i$, where:
$$\alpha(\tau) = \alpha e^{-\tau}, \quad \theta_0(\tau) = \theta_0 e^{-\tau}, \quad \theta_1(\tau) = \theta_1 e^{-\tau}$$
for $\hat{\tau}^k \le T = 30$, with $\theta_0 = \theta_1 = 1$.
3. Use the neural network to output $\log P_i^\tau = \log \hat{P}(\tau_i, W_i, r_i, \beta_i), \eta_{r,i}^\tau = \eta_r(\tau_i, W_i, r_i, \beta_i), \eta_{\beta,i}^\tau = \eta_\beta(\tau_i, W_i, r_i, \beta_i)$, and $\log \nu_i = \log \hat{\nu}(W_i, r_i, \beta_i), \eta_{r,i}^\nu = \eta_r^\nu(W_i, r_i, \beta_i), \eta_{\beta,i}^\nu = \eta_\beta^\nu(W_i, r_i, \beta_i)\}$. Compute the drift term for the bond price with maturity τ_i
$$\omega_i^\tau - r_i = \gamma\left(\eta_{r,i}^\tau\left(\sum_{k=1}^K \hat{x}_t^k \eta_{r,i}^k(\tau^k - \tau^{k-1})\right) + \eta_{\beta,i}^\tau\left(\sum_{k=0}^K \hat{x}_t^k \eta_{\beta,t}^k(\tau^k - \tau^{k-1})\right)\right) - (1-\gamma)\left(\eta_{r,i}^\tau \eta_{r,i}^\nu + \eta_{\beta,i}^\tau \eta_{\beta,i}^\nu\right).$$
To follow the same formula, compute the drift terms ω_i^k for debt of maturity $\hat{\tau}^k, k = 1, \cdots, K$.
4. Compute the drift and volatility terms for aggregate wealth and the drift of ν_t
$$\omega_i = W_i r_i + \xi(\bar{W} - W_i) + \sum_{k=1}^K X_i^k(\omega_i^k - r_i)(\tau^k - \tau^{k-1})$$
$$\eta_{r,i} = \frac{1}{W_i}\sum_{k=1}^K X_i^k \eta_{r,i}^k(\tau^k - \tau^{k-1}) \qquad \eta_{\beta,i} = \frac{1}{W_i}\sum_{k=1}^K X_i^k \eta_{\beta,i}^k(\tau^k - \tau^{k-1})$$
$$\omega_i^\nu = -\left[r_i + \frac{1}{W_i}\sum_{k=1}^K X_i^k(\omega_i^k - r_i)(\tau^k - \tau^{k-1})\right] + \frac{1}{2}\gamma\left[(\eta_{r,i}^\nu)^2 + (\eta_{\beta,i}^\nu)^2 + (\eta_{r,i}^2 + \eta_{\beta,i}^2)\right] - (1-\gamma)\left[\eta_{r,i}\eta_{r,i}^\nu + \eta_{\beta,i}\eta_{\beta,i}^\nu\right] - (\xi + \rho)\frac{\nu_i^{\gamma-1} - 1}{1-\gamma}$$
5. Update $\log P_i^\tau$ and $\log \nu_i$:
$$\log P_{i+1}^\tau = \log P_i^\tau + \left(\omega_i^\tau - \frac{1}{2}(\eta_{r,i}^\tau)^2 - \frac{1}{2}(\eta_{\beta,i}^\tau)^2\right)\Delta + \eta_{r,i}^\tau(B_{r,i+1} - B_{r,i}) + \eta_{\beta,i}^\tau(B_{\beta,i+1} - B_{\beta,i})$$
$$\log \nu_{i+1} = \log \nu_i + \left(\omega_i^\nu - \frac{1}{2}(\eta_{r,i}^\nu)^2 - \frac{1}{2}(\eta_{\beta,i}^\nu)^2\right)\Delta + \eta_{r,i}^\nu(B_{r,i+1} - B_{r,i}) + \eta_{\beta,i}^\nu(B_{\beta,i+1} - B_{\beta,i})$$
6. Update state variables:
$$W_{i+1} = W_i + \omega_i\Delta + \eta_{r,i}(B_{r,i+1} - B_{r,i}) + \eta_{\beta,i}(B_{\beta,i+1} - B_{\beta,i})$$
$$\tau_{i+1} = \tau_i - \Delta$$

$$r_{i+1} = r_i + \kappa_r(\bar{r} - r_i)\Delta + \sigma_r(B_{r,i+1} - B_{r,i})$$

$$\beta_{i+1} = \beta_i - \kappa_\beta \beta_i \Delta + \sigma_\beta(B_{\beta,i+1} - B_{\beta,i})$$

7. When $\tau_{i+1} = 0$, stop updating this sample in the time iteration.
8. Use the neural network to output:

$$\log \hat{P}^\tau_{i+1} = \log \hat{P}(\tau_{i+1}, W_{i+1}, r_{i+1}, \beta_{i+1}), \quad \log \hat{\nu}_{i+1} = \log \hat{\nu}(W_{i+1}, r_{i+1}, \beta_{i+1})$$

9. Update the loss:

$$\text{loss} = \text{loss} + \frac{1}{M}\left(\log \hat{P}^\tau_{i+1} - \log P^\tau_{i+1}\right)^2 + \frac{1}{M}\left(\log \hat{\nu}_{i+1} - \log \nu_{i+1}\right)^2$$

Repeat steps 2 to 9 until all **I** time iterations are completed.

3.3 Numerical Results

In this section, we present the key equilibrium features of the model. We begin by analyzing the determinants of the bond risk premium, followed by an examination of how changes in arbitrageurs' wealth levels affect the yield curve.

3.3.1 Decomposition of the Risk Premium

We can reformulate the Euler equation for the bond price as follows:

$$\omega^\tau_t = r_t + \underbrace{\gamma\left[\eta^\tau_{r,t}\left(\int_0^\infty \hat{x}^s_t \eta^s_{r,t}\, ds\right) + \eta^\tau_{\beta,t}\left(\int_0^\infty \hat{x}^s_t \eta^s_{\beta,t}\, ds\right)\right]}_{\text{covariance with portfolio}} - \underbrace{(1-\gamma)\left[\eta^\tau_{r,t}\eta^\nu_{r,t} + \eta^\tau_{\beta,t}\eta^\nu_{\beta,t}\right]}_{\text{intertemporal hedging}} \tag{16}$$

Figure 5 illustrates the decomposition of the bond return ω^τ_t under different states.The figure is arranged in a 3×3 grid, with each cell corresponding to a unique combination of states: rows indicate varying levels of the short rate r (low, medium, high from top to bottom), and columns reflect different values of the demand factor β (negative, zero, positive from left to right). Within each cell, the dashed lines correspond to r_t plus the risk premium with respect to wealth ($r_t + \gamma\left[\eta^\tau_{r,t}\left(\int_0^\infty \hat{x}^s_t \eta^s_{r,t}\, \mathrm{d}s\right) + \eta^\tau_{\beta,t}\left(\int_0^\infty \hat{x}^s_t \eta^s_{\beta,t}\, \mathrm{d}s\right)\right]$ in (16), while the solid lines represent ω^τ_t.

Several observations can be obtained from Figure 5. First, all solid lines lie below the dashed ones, indicating that intertemporal hedging motives reduce the risk premium. Second, higher short interest rates increase the risk premium, as does a higher preference state β. Additionally, under certain conditions—particularly when the short rate r is high and the demand factor β is low—the covariance between a bond's return and the entire portfolio can be negative, with the colored dashed lines falling below the short rate r. This stems from negative portfolio duration and a short position in bonds of specific maturities, as later demonstrated in Figures 6 and 7.

The effect of changes in arbitrageurs' aggregate wealth level differs, depending on the sign of the term premium with respect to the aggregate wealth. A higher wealth level reduces the term premium when it is positive and increases it when negative, as governed by $\hat{x}^s_t = X^s_t / W_t$ in

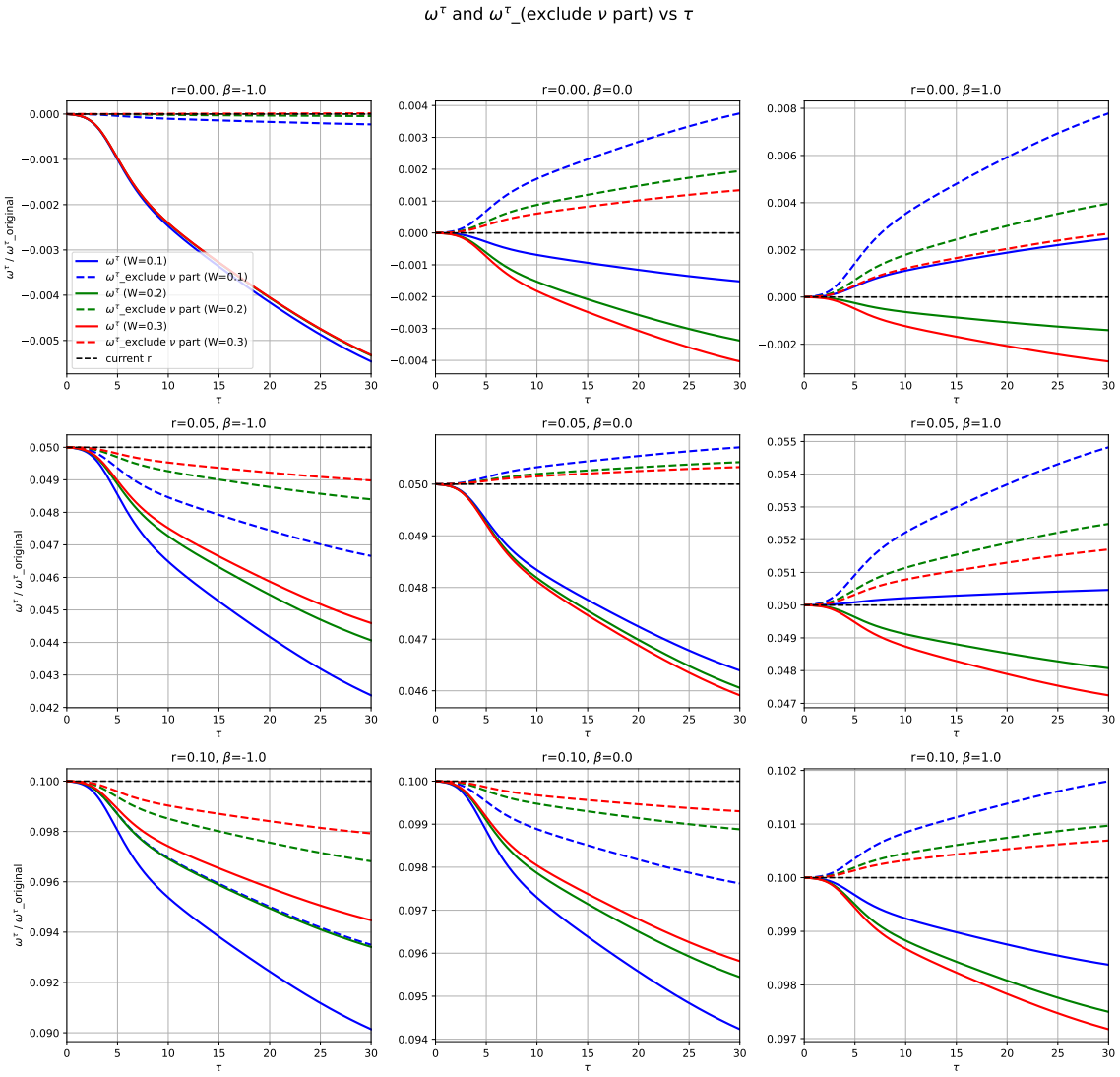

Figure 5: Risk premium.
The figure shows the decomposition of the bond risk premium $\omega_t^\tau - r_t$ across different states. Each cell in the 3×3 grid corresponds to a combination of short rate r (rows: low, medium, high from top to bottom) and preference state β (columns: negative, zero, positive from left to right). The solid lines represent the total ω_t^τ, while the dashed lines indicate r_t plus the risk premium with respect to wealth.

(16). Intuitively, this aligns with the wealth multiplier decreasing with arbitrageurs' aggregate wealth and the empirical observation that greater market liquidity lowers the risk premium.

3.3.2 Portfolio Duration

Figure 6 illustrates the average duration of an arbitrageur's portfolio as a function of the arbitrageurs' wealth W under different combinations of the short rate r and the demand factor β. The average duration in the model is

$$D_t = \frac{\int_0^\infty \tau X_t^{(\tau)} d\tau}{W_t}.$$

The figure is organized as a 3×3 grid, where each cell corresponds to a specific combination of states: the rows represent different levels of the short rate r (0.00, 0.05, 0.10 from top to bottom), and the columns represent different values of the demand factor β (-1.0, 0.0, 1.0 from left to right). Within each cell, the solid lines depict the portfolio duration as W varies from 0.1 to 0.3.

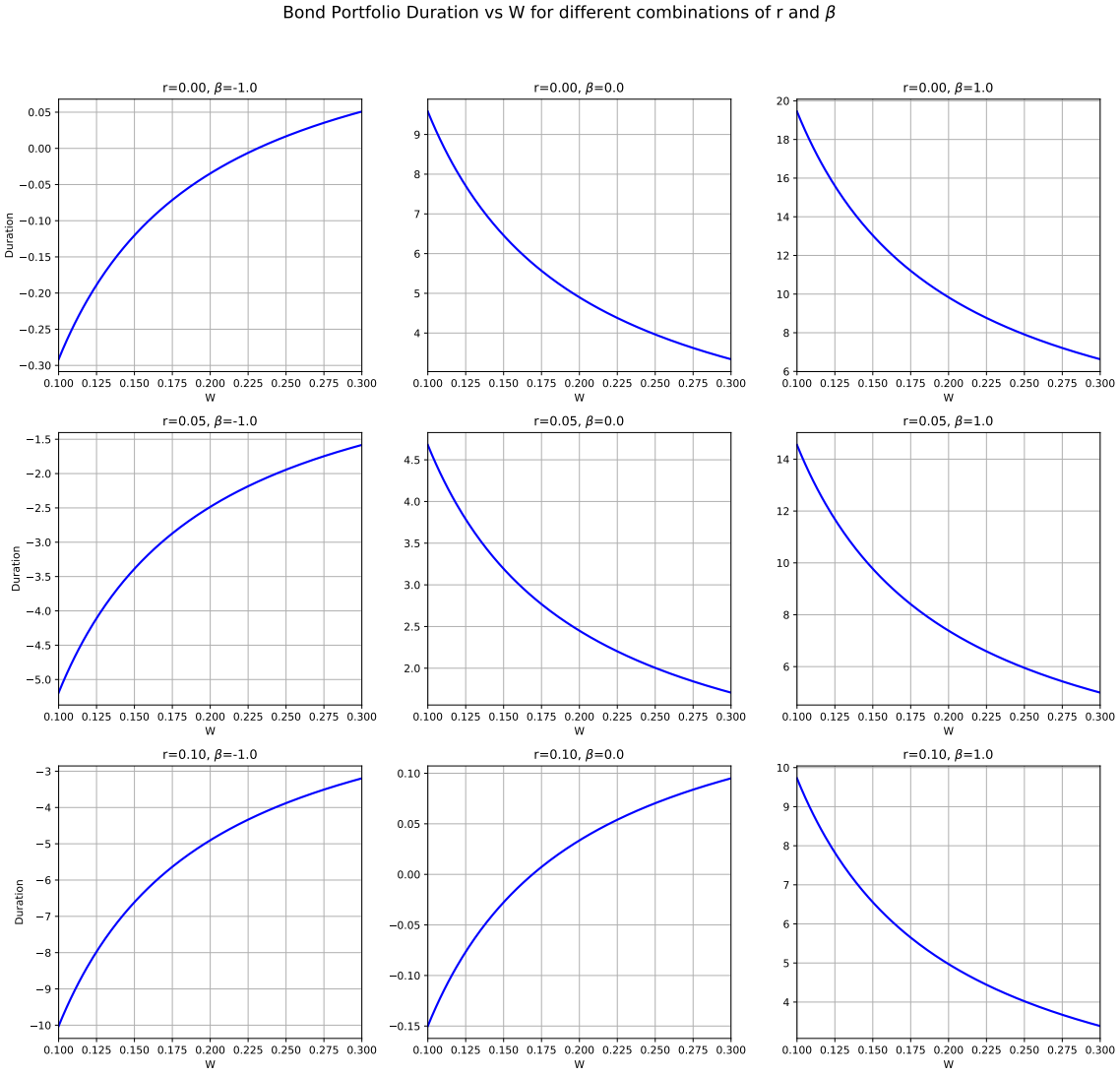

Figure 6: Portfolio duration
This figure shows the portfolio duration as a function of arbitrageurs' aggregate wealth W under different combinations of r and β. Each cell in the 3×3 grid corresponds to a combination of short rate r (rows: 0.00, 0.05, 0.10 from top to bottom) and preference β (columns: -1.0, 0.0, 1.0 from left to right).

Several key insights can be drawn from the figure. First, the portfolio duration is highly sensitive to the values of r and β. Specifically, smaller values of β and higher values of r are associated with lower portfolio durations. In some cases, particularly when β is negative and r is high, the arbitrageurs' portfolio duration becomes negative due to large long positions taken by preferred habitat investors, which in turn leads to a negative term premium (Figure 7). This negative duration implies that the portfolio's value rises as interest rates increase.

3.3.3 Bond Demand Across Different Maturities

Figure 7 shows the bond demand as a function of time to maturity τ across different states and wealth levels. The figure is organized as a 3×3 grid, where the rows represent different levels of the short rate r (0.00, 0.05, 0.10 from top to bottom), and the columns represent different values of the demand factor β ($-1.0, 0.0, 1.0$ from left to right). Within each cell, the lines represent bond demand for different wealth levels: $W = 0.1$ (blue), $W = 0.2$ (green), and $W = 0.3$ (red). The red dots mark the midpoints of the discretized τ intervals used in the numerical computation, corresponding to the average bond demand within each interval.

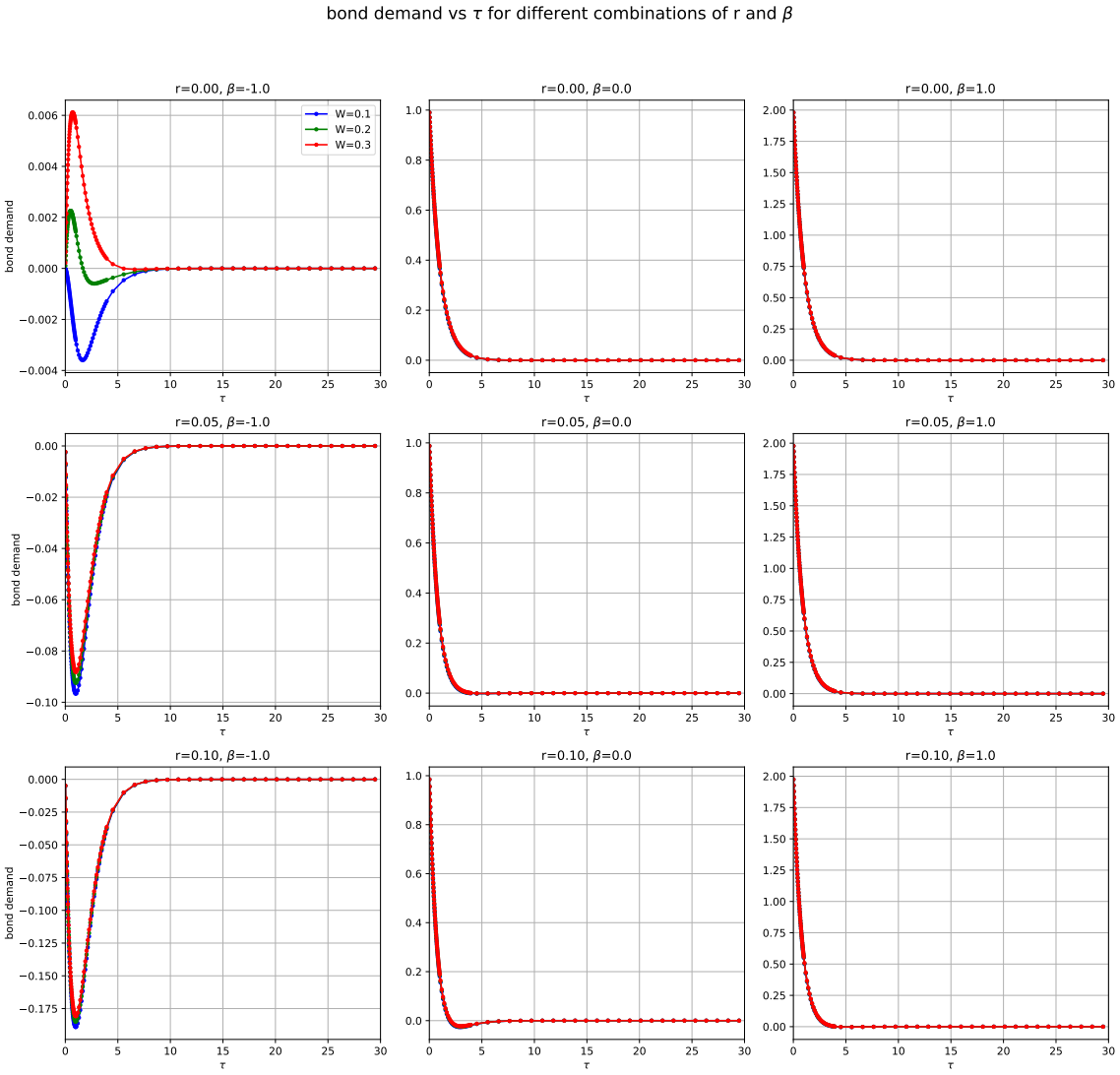

Figure 7: Term structure of aggregate bond demand
This figure shows the term structure of aggregate bond demand under different combinations of r and β. Each cell in the 3×3 grid corresponds to a combination of short rate r (rows: 0.00, 0.05, 0.10 from top to bottom) and demand factor β (columns: -1.0, 0.0, 1.0 from left to right). The lines represent bond demand for wealth levels $W = 0.1$ (blue), $W = 0.2$ (green), and $W = 0.3$ (red). The red dots indicate the midpoints of the discretized τ intervals used in the computation.

3.3.4 Bond Price Sensitivity to Maturity and Short Rate

Figures 8 and 9 present the bond price P as a function of time to maturity τ, short rate r, demand factor β, and wealth levels W. Figure 8 is organized as a 3×3 grid, where the rows represent different levels of the short rate r (0.00, 0.05, 0.10 from top to bottom), and the columns represent different values of the demand factor β ($-1.0, 0.0, 1.0$ from left to right). Within each cell, the lines represent bond prices for different wealth levels: $W = 0.1$ (blue), $W = 0.2$ (green), and $W = 0.3$ (red). Figure 9 is also a 3×3 grid, with rows representing different wealth levels ($W = 0.1$, $W = 0.2$, $W = 0.3$ from top to bottom) and columns representing different β values ($-1.0, 0.0, 1.0$ from left to right). In this figure, the lines represent bond prices for different maturities: $\tau = 1$ (purple), $\tau = 5$ (blue), $\tau = 10$ (cyan), $\tau = 20$ (green), and $\tau = 30$ (yellow), as the short rate r varies from 0.00 to 0.10.

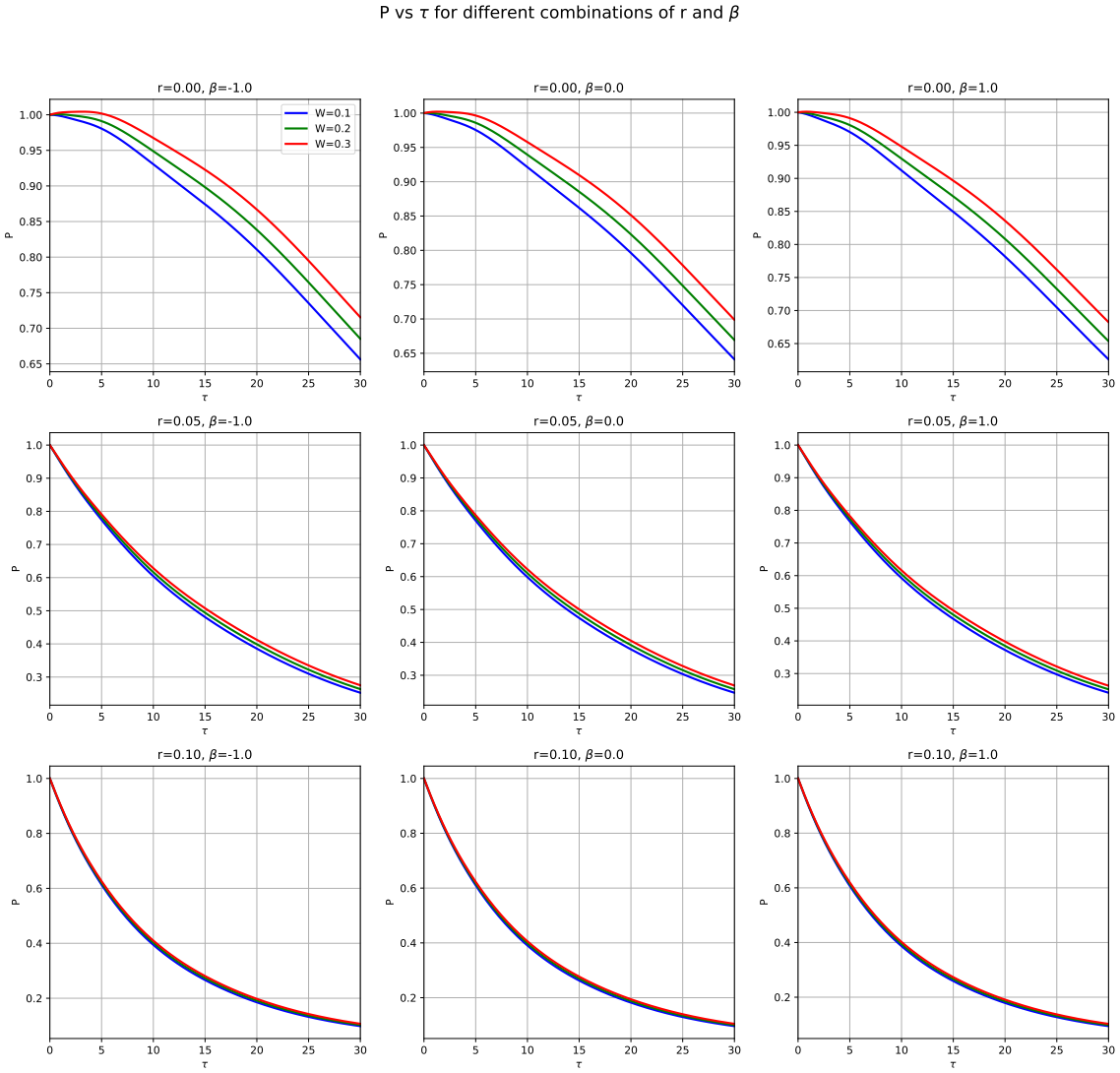

Figure 8: Term structure of bond price
This figure presents the term structure of bond price P under different combinations of r and β. Each cell in the 3×3 grid corresponds to a combination of short rate r (rows: 0.00, 0.05, 0.10 from top to bottom) and demand factor β (columns: $-1.0, 0.0, 1.0$ from left to right). The lines represent bond prices for wealth levels $W = 0.1$ (blue), $W = 0.2$ (green), and $W = 0.3$ (red).

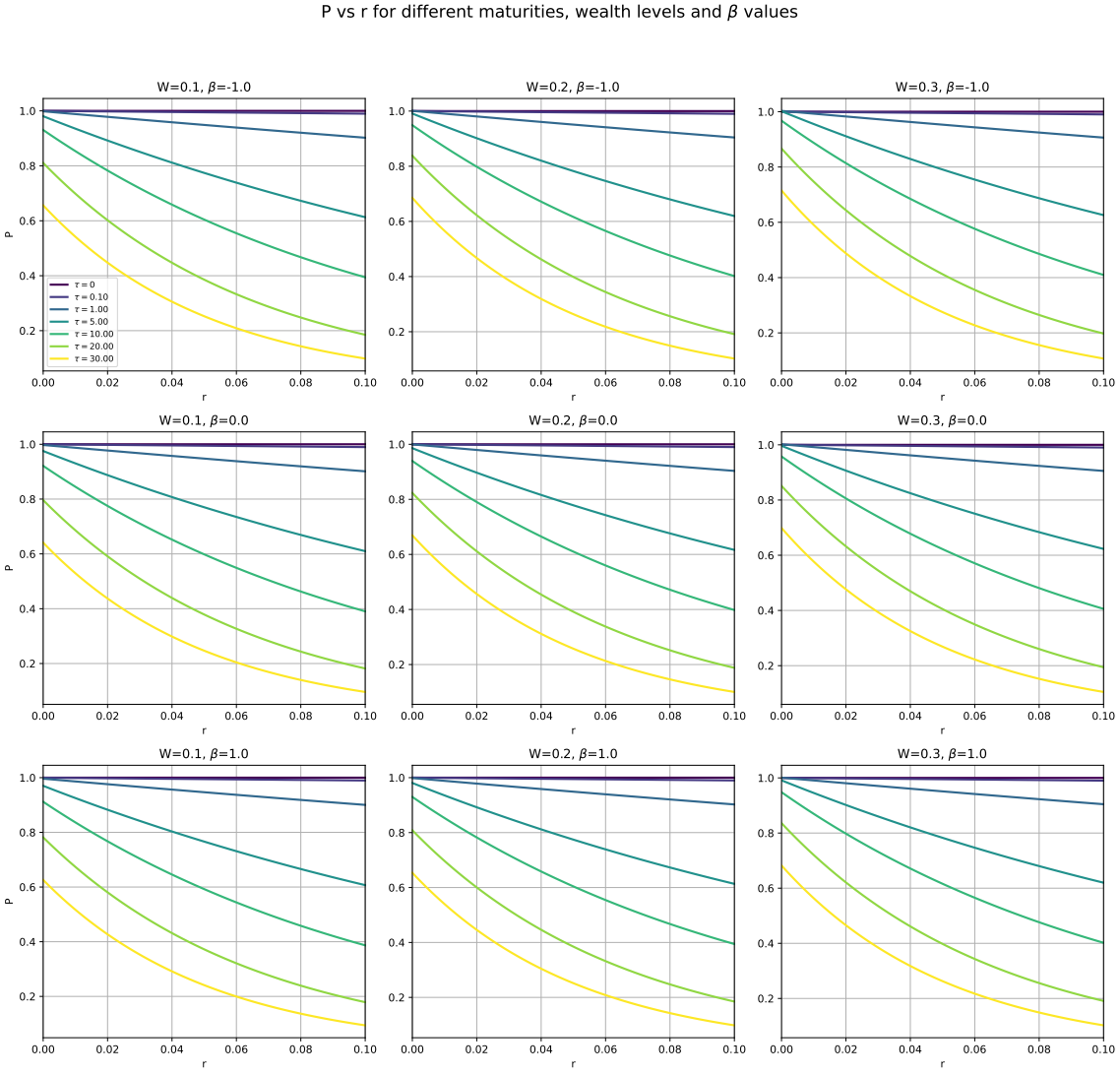

Figure 9: Bond price P against short rate r
This figure presents bond price as a function of the short rate under different maturities, wealth levels, and β values. Each cell in the 3×3 grid corresponds to a combination of wealth W (rows: 0.1, 0.2, 0.3 from top to bottom) and demand factor β (columns: -1.0, 0.0, 1.0 from left to right). The lines represent bond prices for maturities $\tau = 1$ (purple), $\tau = 5$ (blue), $\tau = 10$ (cyan), $\tau = 20$ (green), and $\tau = 30$ (yellow), as r varies from 0.00 to 0.10.

In Figure 8, the bond price P decreases as the time to maturity τ increases across all states, reflecting the discounting effect of longer maturities. Higher wealth levels W result in higher bond prices. This is intuitive, as in (16), $\hat{x}_t^s = X_t^s/W_t$, implying that greater wealth reduces the risk premium and the marginal utility of wealth. Higher short rates r (moving down the rows in Figure 8) significantly lower bond prices, as anticipated due to stronger discounting. For instance, at $r = 0.10$, bond prices fall to approximately 0.2-0.4 for $\tau = 30$, compared to 0.6-0.7 at $r = 0.00$.

Figure 9 confirms the inverse relationship between bond prices and the short rate r. As r rises from 0.00 to 0.10, bond prices decline across all maturities, with longer maturities ($\tau = 30$, yellow) showing a steeper drop than shorter ones ($\tau = 1$, purple), consistent with the greater sensitivity of long-term bonds to interest rate changes.

In Figure 9, the influence of β is evident: positive β values (right column) yield higher bond prices across all maturities and wealth levels compared to negative β values (left column). Additionally, bond price curves rise with higher arbitrageurs' aggregate wealth W (comparing curves across columns).

3.3.5 Wealth Multiplier across Different States

Figure 10 illustrates the wealth multiplier ν as a function of the arbitrageurs' wealth W across different combinations of the short rate r and the demand factor β. The figure is organized as a 3×3 grid, where each cell corresponds to a specific combination of states: the rows represent different levels of the short rate r (0.00, 0.05, 0.10 from top to bottom), and the columns represent different values of the demand factor β ($-1.0, 0.0, 1.0$ from left to right).

Figure 10 shows that as arbitrageurs' total wealth increases, the wealth multiplier ν — the present value of future investment opportunity — declines as the bond price is higher as the financial intermediary sector is better capitalized (Figure **??**). For a similar reason, when the short rate increases, the bond price declines and the value of future investment opportunities appreciate, which leads to a higher wealth multiplier (comparing upper panels with lower ones).

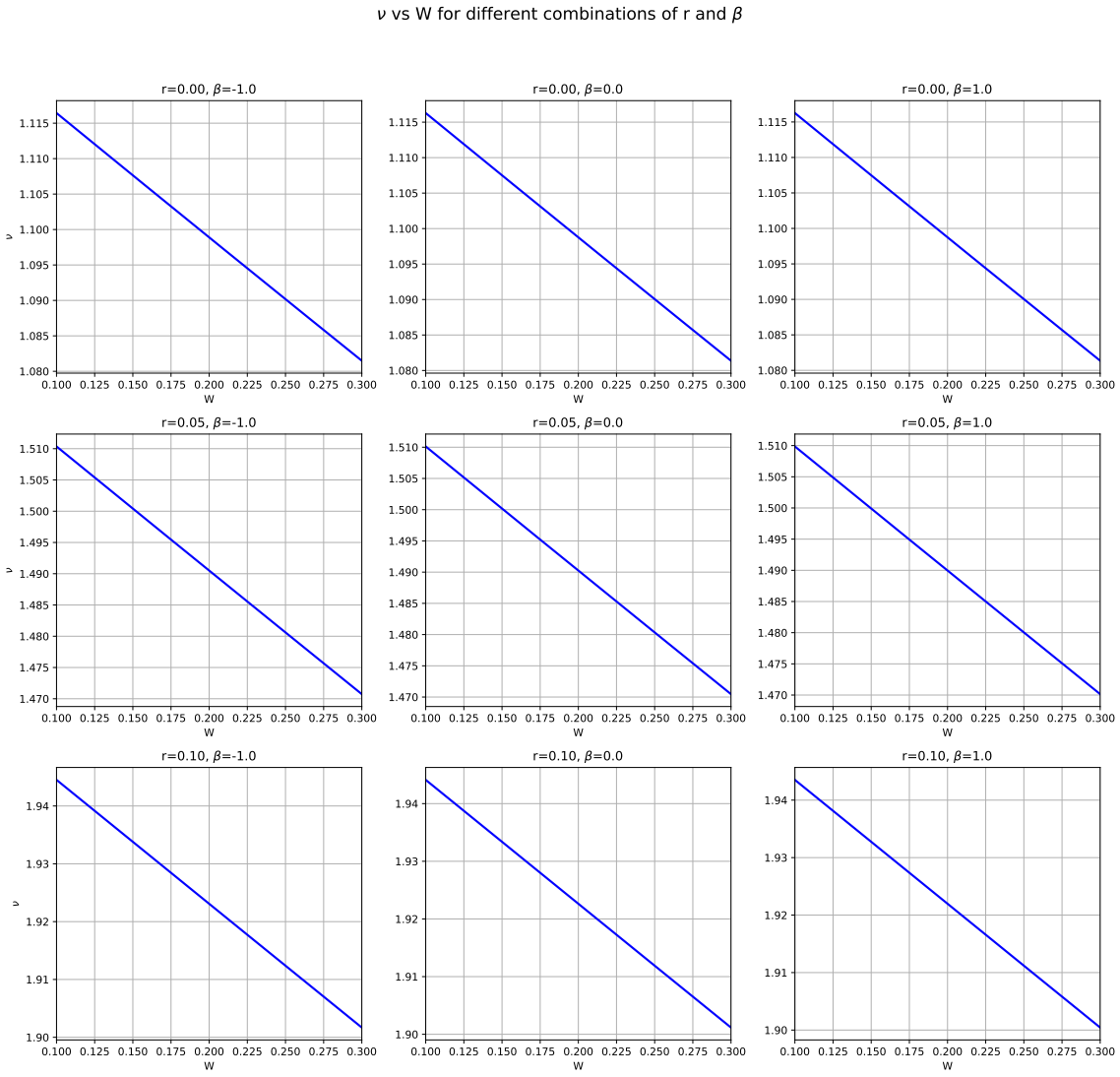

Figure 10: Wealth multiplier ν
This figure shows the wealth multiplier as a function of arbitrageurs' aggregate wealth W under different combinations of r and β. Each cell in the 3×3 grid corresponds to a combination of short rate r (rows: 0.00, 0.05, 0.10 from top to bottom) and preference β (columns: $-1.0, 0.0, 1.0$ from left to right).

3.3.6 Volatility of Bond Price and Marginal Value

Figures 11 and 12 illustrate the volatility terms of the bond price (η_r^τ, η_β^τ) and the marginal value (η_r^ν, η_β^ν) with respect to the Brownian motions $\mathrm{d}B_{r,t}$ and $\mathrm{d}B_{\beta,t}$, respectively, across different states and wealth levels. Each figure is organized as a 3×3 grid, where the rows represent different levels of the short rate r (0.00, 0.05, 0.10 from top to bottom), and the columns represent different values of the demand factor β ($-1.0, 0.0, 1.0$ from left to right). Within each cell, the solid lines (on the primary y-axis, left) represent η_r^τ or η_β^τ, while the dashed lines (on the secondary y-axis, right) represent η_r^ν or η_β^ν. The colors indicate different wealth levels: $W = 0.1$ (blue), $W = 0.2$ (green), and $W = 0.3$ (red).

First, the volatility terms of bonds across all maturities are negative and decrease with time-to-maturity, indicating that bond prices fall with a positive interest rate shock, with longer-maturity bonds showing a stronger response. The volatility of the wealth multiplier (secondary

y-axis, right) remains positive across all nine scenarios. Higher interest rates, lower wealth levels, and lower demand states result in a reduced response to the interest rate shock. Regarding the volatility terms of both bond prices and the wealth multiplier with respect to the demand shock β in 12, the results are similar to those for the interest rate shock.

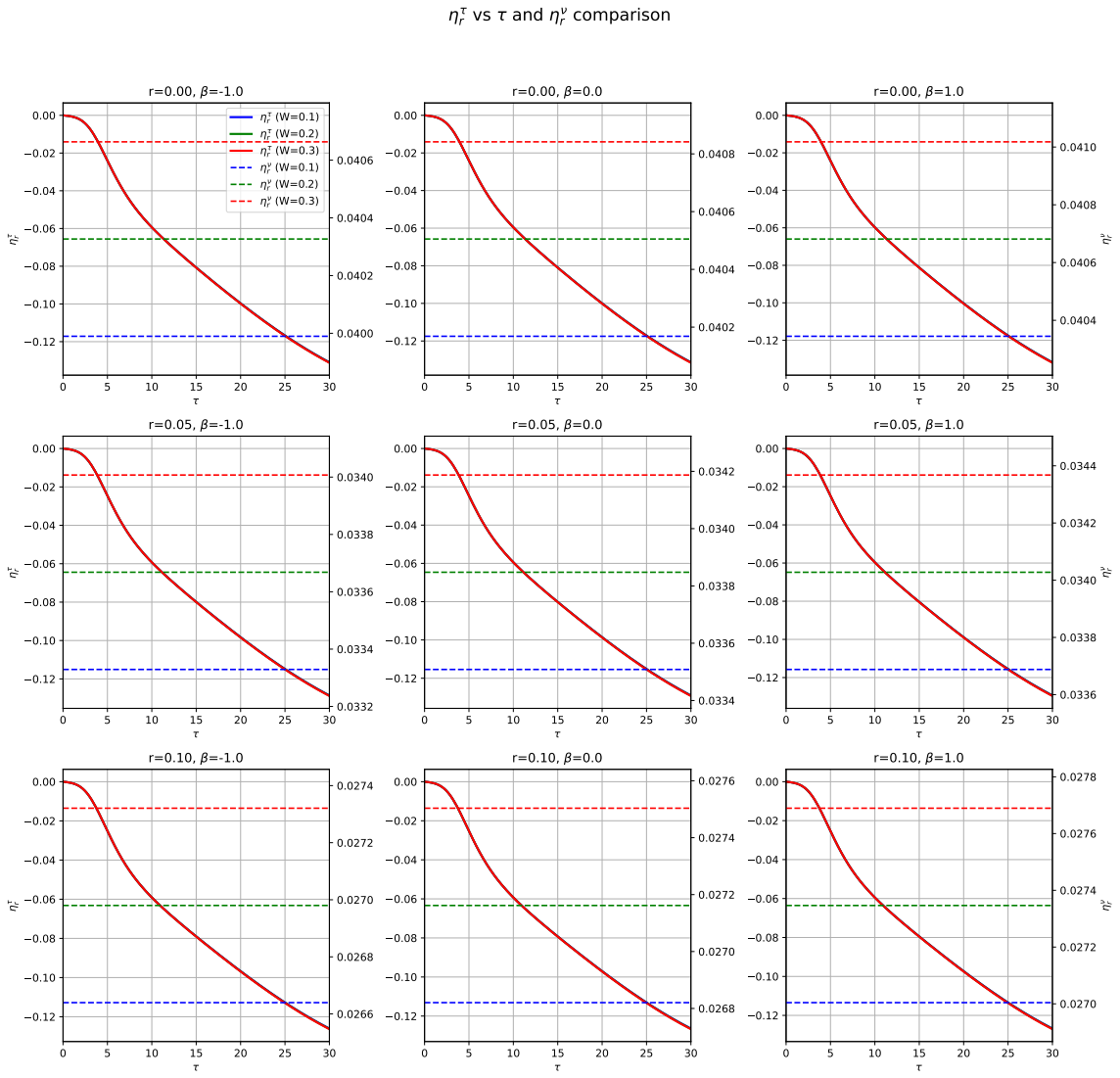

Figure 11: Exposure to short rate risk
This figure presents the term structure of risk exposure to the short rate shock, η_r^τ and η_r^ν, under different states and wealth levels. Each cell in the 3×3 grid corresponds to a combination of short rate r (rows: 0.00, 0.05, 0.10 from top to bottom) and demand factor β (columns: $-1.0, 0.0, 1.0$ from left to right). The solid lines (primary y-axis, left) represent η_r^τ, and the dashed lines (secondary y-axis, right) represent η_r^ν for wealth levels $W = 0.1$ (blue), $W = 0.2$ (green), and $W = 0.3$ (red).

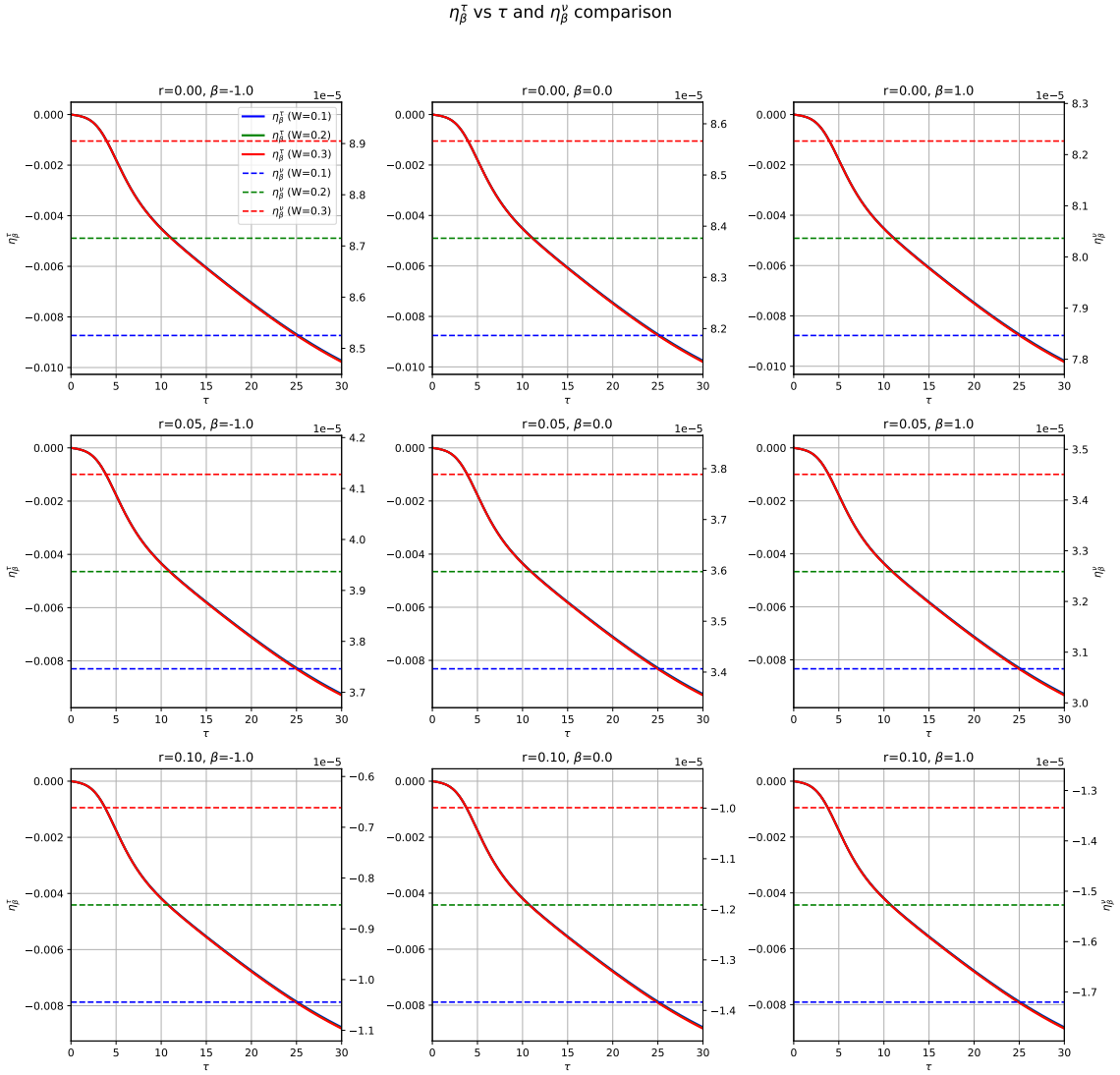

Figure 12: Exposure to demand risk
This figure presents the term structure of risk exposure to demand shocks, η_β^τ and η_β^ν, across different states and wealth levels. Each cell in the 3×3 grid corresponds to a combination of short rate r (rows: 0.00, 0.05, 0.10 from top to bottom) and demand factor β (columns: -1.0, 0.0, 1.0 from left to right). The solid lines (primary y-axis, left) represent η_β^τ, and the dashed lines (secondary y-axis, right) represent η_β^ν for wealth levels $W = 0.1$ (blue), $W = 0.2$ (green), and $W = 0.3$ (red).

3.3.7 Dynamics of Aggregate Wealth

Figures 13 and 14 present the drift and volatility terms of arbitrageurs' aggregate wealth W across different states. Figure 13 shows the drift term ω^W as a function of wealth W, while Figure 14 shows the volatility terms η_r^W (with respect to the r-shock, $B_{r,t}$) and η_β^W (with respect to the β-shock, $B_{\beta,t}$). Both figures are organized as 3×3 grids, where the rows represent different levels of the short rate r (0.00, 0.05, 0.10 from top to bottom), and the columns represent different values of the demand factor β ($-1.0, 0.0, 1.0$ from left to right). In Figure 14, the solid blue lines (primary y-axis, left) represent η_r^W, while the red dashed lines (secondary y-axis, right) represent η_β^W.

In Figure 13, the drift term ω^W exhibits different behaviors under different combinations of

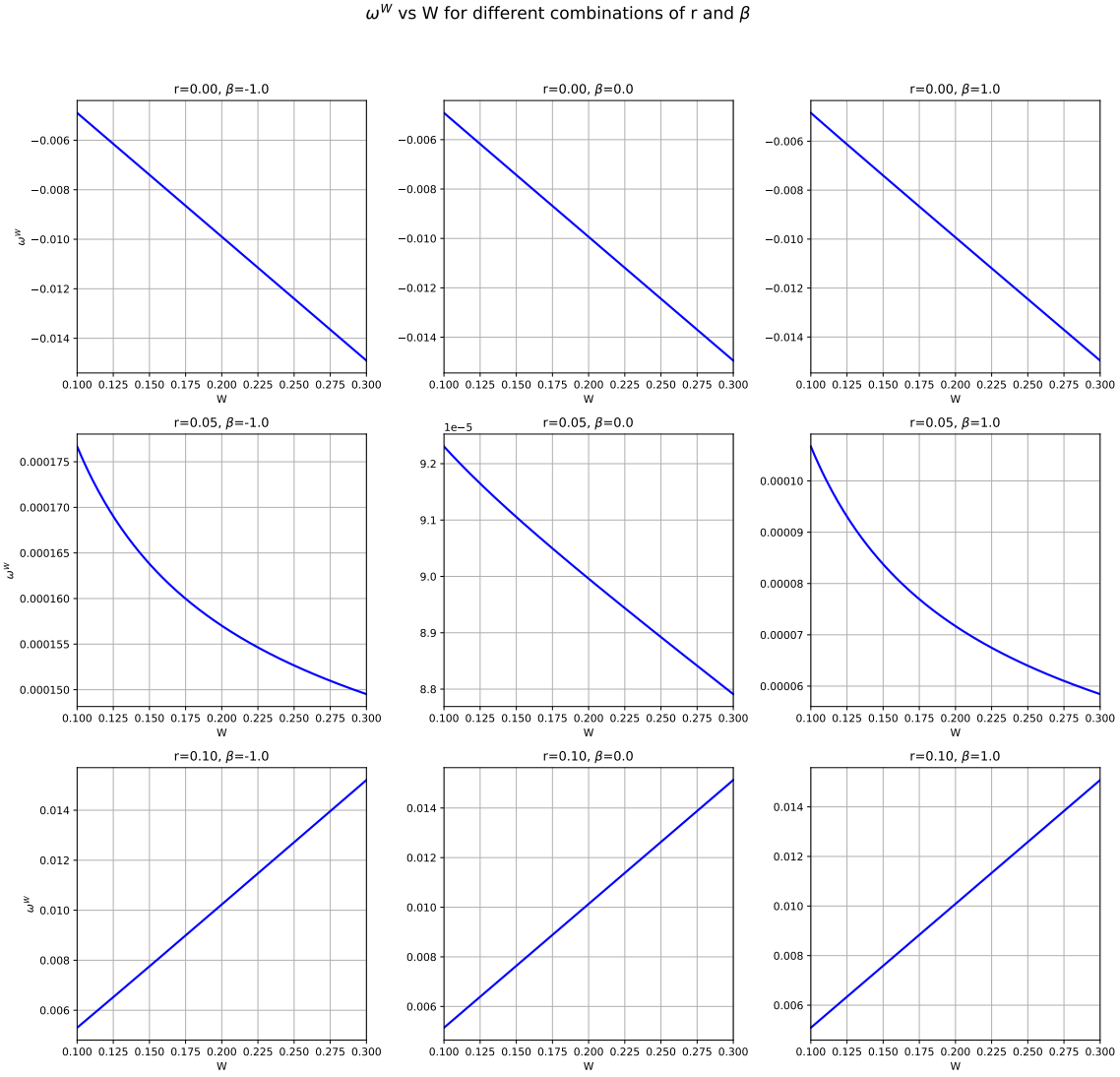

Figure 13: Drift of arbitrageurs' total wealth ω^W
This figure presents the drift term of arbitrageurs' total wealth ω^W against its level W under different combinations of r and β. Each cell in the 3×3 grid corresponds to a combination of short rate r (rows: 0.00, 0.05, 0.10 from top to bottom) and demand factor β (columns: -1.0, 0.0, 1.0 from left to right).

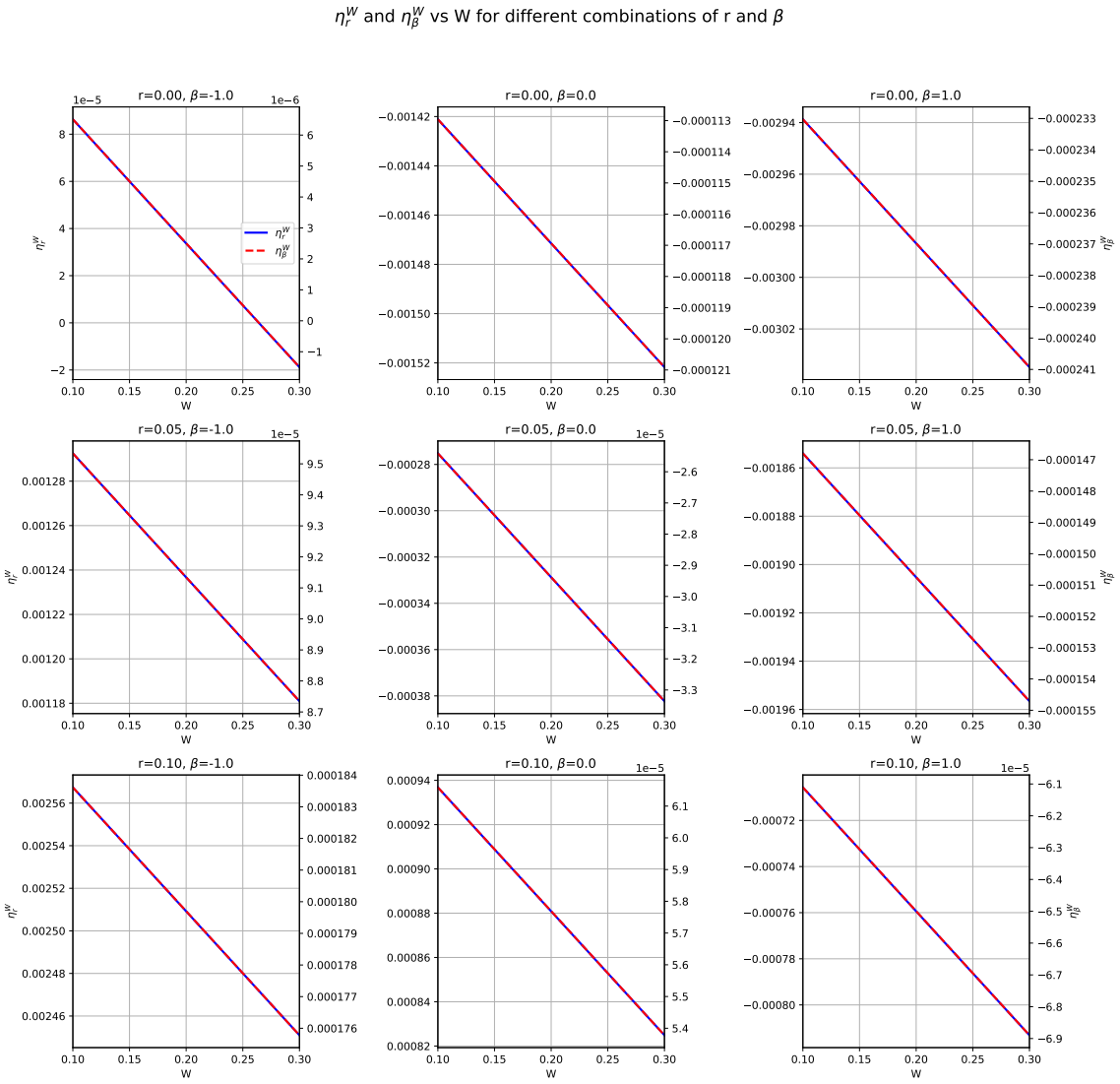

Figure 14: Volatility of arbitrageurs' total wealth ω^W

This figure presents the drift term of arbitrageurs' total wealth ω^W against its level W under different combinations of r and β. Each cell in the 3×3 grid corresponds to a combination of short rate r (rows: 0.00, 0.05, 0.10 from top to bottom) and demand factor β (columns: -1.0, 0.0, 1.0 from left to right). The solid blue lines (primary y-axis, left) represent η_r^W, and the red dashed lines (secondary y-axis, right) represent η_β^W.

the short rate r and demand factor β. For lower r (e.g., $r = 0.00$), ω^W is negative and declines as W increases, indicating a tendency for aggregate wealth to decrease. Conversely, for higher r (e.g., $r = 0.10$), ω^W becomes positive and increases with W, suggesting wealth growth. The demand factor β also influences the drift of W_t : a positive β (e.g., $\beta = 1.0$) generally yields a less negative or more positive ω^W compared to a negative β (e.g., $\beta = -1.0$), reflecting the impact of investor preferences on wealth dynamics.

In Figure 14, the volatility term η_r^W (solid blue lines, primary y-axis) is negative and decreases as the arbitrageurs' total wealth W increases, indicating that the sensitivity of wealth to interest rate shocks diminishes with higher wealth levels. The magnitude of η_r^W is relatively stable across different r and β values, exhibiting low sensitivity to these state variables. Similarly, the volatility term η_β^W (red dashed lines, secondary y-axis) is negative and declines with W.

4 Final Remarks

In this paper, we outline a class of economic models with high-dimensional controls that are numerically solvable using a deep learning-based probabilistic approach. Specifically, the number of function evaluations is proportional to the dimensionality of the controlled state variable, $O(N)$, as opposed to its square, $O(N^2)$. The second coauthor has applied this approach to models with high-dimensional, uncontrolled aggregate state variables (Huang, 2023b,a). However, an important class of models remains uncovered by the probabilistic approach—those with state variables that include forward-looking components.

A prominent example is the Ramsey problem, in which individual agents' optimality conditions must be satisfied while the social planner controls the law of motion for aggregate state variables. Similarly, there are numerous examples in the study of repeated and stochastic games.

We speculate that combining the Negishi method, as advocated in Bloise and Siconolfi (2022), with the probabilistic formulation in the continuous-time setting could be a promising direction for addressing forward-looking constraints. Currently, Faingold and Sannikov (2020) are addressing stochastic games with moral hazard problems in the continuous-time setting using the analytic/PDE method, whose convex analysis shares significant similarities with the Negishi method.

References

Aiyagari, S Rao, Albert Marcet, Thomas J Sargent, and Juha Seppälä (2002) "Optimal taxation without state-contingent debt," *Journal of Political Economy*, Vol. 110, pp. 1220–1254.

Angeletos, George-Marios (2002) "Fiscal policy with noncontingent debt and the optimal maturity structure," *The Quarterly Journal of Economics*, Vol. 117, pp. 1105–1131.

Arellano, Cristina and Ananth Ramanarayanan (2012) "Default and the maturity structure in sovereign bonds," *Journal of Political Economy*, Vol. 120, pp. 187–232.

Bigio, Saki, Galo Nuno, and Juan Passadore (2023) "Debt-maturity management with liquidity costs," *Journal of Political Economy Macroeconomics*, Vol. 1, pp. 119–190.

Bloise, Gaetano and Paolo Siconolfi (2022) "A Negishi Approach to Recursive Contracts," *Econometrica*, Vol. 90, pp. 2821–2855.

Brunnermeier, Markus K and Motohiro Yogo (2009) "A note on liquidity risk management," *American Economic Review*, Vol. 99, pp. 578–583.

DeMarzo, Peter M and Zhiguo He (2021) "Leverage dynamics without commitment," *The Journal of Finance*, Vol. 76, pp. 1195–1250.

Faingold, Eduardo and Yuliy Sannikov (2020) "Moral hazard in stochastic differential games: Beyond markov equilibrium," *Unpublished working paper*.

Faraglia, Elisa, Albert Marcet, Rigas Oikonomou, and Andrew Scott (2019) "Government debt management: The long and the short of it," *The Review of Economic Studies*, Vol. 86, pp. 2554–2604.

Gourinchas, Pierre-Olivier, Walker Ray, and Dimitri Vayanos (2022) "A preferred-habitat model of term premia, exchange rates, and monetary policy spillovers,"Technical report, National Bureau of Economic Research.

Guibaud, Stéphane, Yves Nosbusch, and Dimitri Vayanos (2013) "Bond market clienteles, the yield curve, and the optimal maturity structure of government debt," *The Review of Financial Studies*, Vol. 26, pp. 1914–1961.

Han, Jiequn, Arnulf Jentzen, and Weinan E (2018) "Solving high-dimensional partial differential equations using deep learning," *Proceedings of the National Academy of Sciences*, Vol. 115, pp. 8505–8510.

He, Zhiguo and Konstantin Milbradt (2016) "Dynamic debt maturity," *The Review of Financial Studies*, Vol. 29, pp. 2677–2736.

Huang, Ji (2023a) "Breaking the Curse of Dimensionality in Heterogeneous-Agent Models: A Deep Learning-Based Probabilistic Approach," *Available at SSRN 4649043*.

——— (2023b) "A Probabilistic Solution to High-Dimensional Continuous-Time Macro and Finance Models."

Kekre, Rohan, Moritz Lenel, and Federico Mainardi (2024) "Monetary policy, segmentation, and the term structure,"Technical report, National Bureau of Economic Research.

Lustig, Hanno, Christopher Sleet, and Şevin Yeltekin (2008) "Fiscal hedging with nominal assets," *Journal of Monetary Economics*, Vol. 55, pp. 710–727.

Pardoux, Etienne and Shige Peng (1990) "Adapted solution of a backward stochastic differential equation," *Systems & Control Letters*, Vol. 14, pp. 55–61.

Ray, Walker, Michael Droste, and Yuriy Gorodnichenko (2024) "Unbundling quantitative easing: Taking a cue from treasury auctions," *Journal of Political Economy*, Vol. 132, pp. 3115–3172.

Valaitis, Vytautas and Alessandro T Villa (2024) "A machine learning projection method for macro-finance models," *Quantitative Economics*, Vol. 15, pp. 145–173.

Vayanos, Dimitri and Jean-Luc Vila (2021) "A preferred-habitat model of the term structure of interest rates," *Econometrica*, Vol. 89, pp. 77–112.

Appendix

A Numerical Scheme for Bond Pricing in Section 2

Generate a large number of initial states $\{\tau_0^m, r_0^m\}$, where m is the index for each path that will be dropped as the calculation for all paths are identical. Use a neural network to approximate $\psi(\tau, r)$ denoted as $\psi(\tau, r; \Theta)$, which yields $\psi_0 = \psi(\tau_0, r_0; \Theta)$. We also have a neural network $\sigma^\psi(\tau, r; \Theta)$. With $\tau_i > 0$, r_i, and ψ_i, update them as

$$\begin{aligned}
\tau_{i+1} &= \tau_i - \Delta \\
r_{i+1} &= r_i + \kappa(\theta - r_i)\Delta + \sigma^r \sqrt{r_i}(W_{i+1} - W_i) \\
\psi_{i+1} &= \psi_i + (r_i\psi_i - \delta)\Delta + \sigma^\psi(\tau_i, r_i)(W_{i+1} - W_i)
\end{aligned}$$

Keep track of the loss:

$$\text{Loss} = \text{Loss} + \frac{1}{MN}\sum_{m=1}^{N}\left(\psi_i - \psi(\tau_i, r_i; \Theta)\right)^2$$

If $\tau_N = 0$, then $\psi(\tau_N, r_N; \Theta) = 1$. The boundary condition is not put into the loss function but is implicitly realized through the following transformation. Let the multi-layer perceptron output $\tilde{\psi}(\tau_i, r_i; \Theta)$, and let

$$\psi(\tau_i, r_i; \Theta) \equiv (1 - p(\tau)) \times 1 + p(\tau) \times \tilde{\psi}(\tau_i, r_i; \Theta),$$

where

$$p(\tau) = \sin\left(\frac{\pi}{2} \times \frac{\tau}{T}\right)$$